SANDIA REPORT

SAND2009-7527
Unlimited Release
Printed November 2009

Ferroelectric Opening Switches for Large-Scale Pulsed Power Drivers

Kim Reed, Joe Rudys, Gary Peña, Steve Glover, Geoffrey Brennecka, Bruce Tuttle

Prepared by
Sandia National Laboratories
Albuquerque, New Mexico 87185 and Livermore, California 94550

Sandia is a multiprogram laboratory operated by Sandia Corporation,
a Lockheed Martin Company, for the United States Department of Energy's
National Nuclear Security Administration under Contract DE-AC04-94AL85000.

Sandia National Laboratories

Issued by Sandia National Laboratories, operated for the United States Department of Energy by Sandia Corporation.

Printed in the United States of America. This report has been reproduced directly from the best available copy.

Available to DOE and DOE contractors from
U.S. Department of Energy
Office of Scientific and Technical Information
P.O. Box 62
Oak Ridge, TN 37831

Telephone:	(865) 576-8401
Facsimile:	(865) 576-5728
E-Mail:	reports@adonis.osti.gov
Online ordering:	http://www.osti.gov/bridge

Available to the public from
U.S. Department of Commerce
National Technical Information Service
5285 Port Royal Rd.
Springfield, VA 22161

Telephone:	(800) 553-6847
Facsimile:	(703) 605-6900
E-Mail:	orders@ntis.fedworld.gov
Online order:	http://www.ntis.gov/help/ordermethods.asp?loc=7-4-0#online

SAND2009-7527
Unlimited Release
Printed November 2009

Ferroelectric Opening Switches for Large-Scale Pulsed Power Drivers

K. W. Reed, J. M. Rudys, Gary Peña & S. F. Glover
Advanced Pulsed Power Systems

G. L. Brennecka & B. A. Tuttle
Nanomaterials Sciences

Sandia National Laboratories
P.O. Box 5800
Albuquerque NM 87185-1152

Abstract

Fast electrical energy storage or Voltage-Driven Technology (VDT) has dominated fast, high-voltage pulsed power systems for the past six decades. Fast magnetic energy storage or Current-Driven Technology (CDT) is characterized by 10,000 X higher energy density than VDT and has a great number of other substantial advantages, but it has all but been neglected for all of these decades. The uniform explanation for neglect of CDT technology is invariably that the industry has never been able to make an effective opening switch, which is essential for the use of CDT. Most approaches to opening switches have involved plasma of one sort or another. On a large scale, gaseous plasmas have been used as a conductor to bridge the switch electrodes that provides an opening function when the current wave front propagates through to the output end of the plasma and fully magnetizes the plasma – this is called a Plasma Opening Switch (POS)[1]. Opening can be triggered in a POS using a magnetic field to push the plasma out of the A-K gap – this is called a Magnetically Controlled Plasma Opening Switch (MCPOS).[2] On a small scale, depletion of electron plasmas in semiconductor devices is used to affect opening switch behavior, but these devices are relatively low voltage and low current compared to the hundreds of kilo-volts and tens of kilo-amperes of interest to pulsed power.[3, 4]

This work is an investigation into an entirely new approach to opening switch technology that utilizes new materials in new ways. The new materials are Ferroelectrics and using them as an opening switch is a stark contrast to their traditional applications in optics and transducer applications. Emphasis is on use of high performance ferroelectrics with the objective of developing an opening switch that would be suitable for large scale pulsed power applications. Over the course of exploring this new ground, we have discovered new behaviors and properties of these materials that were here to fore unknown. Some of these unexpected discoveries have lead to new research directions to address challenges.

Acknowledgment

The authors wish to thank the Jeff Alexander, Paul Primm, Mike Horry, Joshua Usher and James Carroll for helping us conduct experiments and collect the data and for their many invaluable suggestions. The authors wish to thank Edward Barnat , Christopher Diantonio and Tom Chavez for their help and scientific expertise in the areas of physics and materials science on the project. The authors wish to thank Ralph (Dave) Clovis, Lance Lippert and Lonnie Martin at the Sandia National Laboratories Annular Core Research Reactor for expediting the neutron irradiation of key materials for this research.

This work was supported by the United States Department of Energy under contract DE-AC04-94ACAC85000.

Contents

APPENDICES:

1.0 Introduction

Magnetic Energy Storage

> "A reliable high-voltage high-current opening switch is required, in order for inductive energy storage to be possible."
>
> . . . This statement or a variation on its theme is invariably in the introduction of nearly every paper reviewed on inductive energy storage.

1.1 <u>Magnetic Energy Storage (MES) energy density is higher than Electric Energy Storage (EES)</u>

The literature sites energy densities[5, 6, 7, 8] in high-voltage (~100 kV) pulse discharge (~100 ns) capacitors as high as 0.26 J/cm^3. Lower voltage (~6.68 kV), slow discharge (~180 us) capacitors are available with energy densities as high as 2.68 J/cm^3[7]. An alternative to capacitive energy storage is inductive energy storage. Conventional inductive storage densities of ~5 J/cm^3 and superconducting inductive energy storage (SCIES) densities of ~50 J/cm^3 are quoted in the literature[5]. An example SCIES design that was built at the Grenoble High Magnetic Field Laboratory stores 26 J/cm^3 based upon the winding volume alone[9]. Energy densities for superconducting inductors (SCI) are complicated by the considerable volume of support equipment that must be included in the effective energy density calculations[10]. Critical current densities as high as 200 kA/cm^2 and critical tangential magnetic flux fields as high as 110 T are possible for *low-temperature* superconductors (SC) in the laboratory[11], and commercial *high-temperature* production tapes are available with critical current densities of 38 kA/cm^2[12]. Thus, these aren't significant limiting factors for SC inductive energy storage (SCIES). The disadvantages of SCIES include that SC materials are costly; support systems are complex, bulky and substantially increase initial and ongoing maintenance expenses. To avoid constant replacement of the expensive liquid helium and nitrogen, the cryogens must run around the clock. It will be shown that the energy lost to heating in a pulse-charged conventional storage inductor is less than 2% of the stored energy with stainless steel electrodes, and can be made as low as 0.25% with copper electrodes. Unless it is necessary to store energy inductively for long times, the benefit of SCs in pulsed power are minimal. For these reasons, SCIES will not be considered further for fast discharge pulsed power in this discussion.

Energy densities sited in the literature are usually taken from particular designs – as are the values given above, rendering the numbers more of a benchmark of what *has* been done than what *can* be done. Energy density numbers in the literature for capacitors are closer to what is *achievable* than those for inductors. The reason is that important high-volume capacitor industry customers have been funding research on capacitor development for decades, particularly for high energy density in low voltage (few kV) and slow discharge (~1 ms) capacitors[7]. The pulsed power community represents a very small part of the capacitor industry's demand, so development of high-energy-density in high-voltage, fast-discharge capacitors has been less aggressive.

To *first order*, it is obvious why the energy density in magnetic fields tends to be so much greater than that in electric fields. If we make a simple comparison of the energy stored in the two fields,

$$\tfrac{1}{2}\,\varepsilon_o E^2 \textit{ versus } \tfrac{1}{2}\mu_o H^2$$

With high electric and magnetic fields, nonlinear high-permittivity (ferroelectrics) and nonlinear hi-permeability (ferromagnetics) materials are not practical for the ultimate in high density energy storage because they saturate at low fields. In the high energy density capacitor industry, the relationship between ferroelectric polarization and applied electric field, known as the P-E curve, is intentionally degraded to yield a relatively linear behavior with typical relative dielectric constants of only about 100. Therefore, a reasonable ball park comparison can be obtained by limiting consideration to the vacuum case,

$$\mu_o \sim 10^5 \text{ x } \varepsilon_o$$

In pulse power systems we routinely use currents of a few Mega-Amperes, so if we use that current in an inductor with a conductor that is 1 meter wide then we can easily get magnetic fields of a few Mega-Ampere-Turns. In pulsed power systems we typically keep electric fields below a few hundred kV/cm or a few 10^7V/m, unless magnetic insulation is used. Magnetic insulation is only used, however, where the energy is predominantly being stored in the form of magnetic fields. So for energy storage applications,

$$H \sim 0.1 \text{ x } E$$

Magnetic energy densities are just naturally about *1000*X higher than electric energy densities. Using a more rigorous approach, the magnetic energy density that one can achieve in a pulsed inductive store is limited by three main factors.

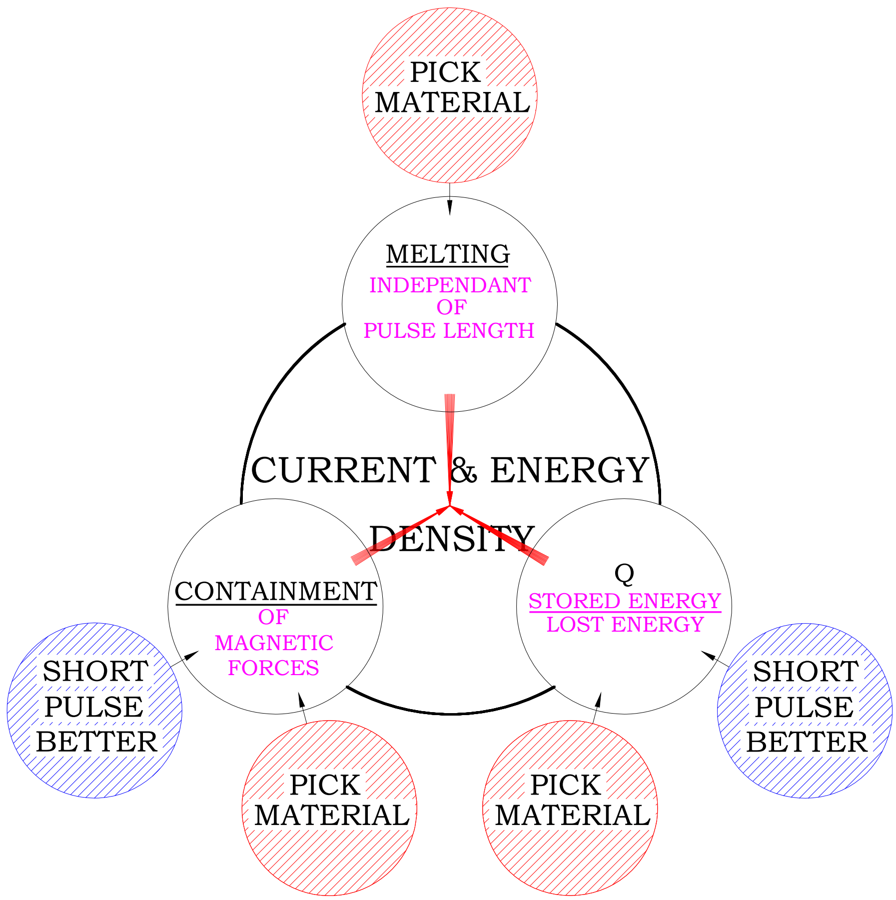

Fig. 1. Melting, Containment & Losses govern the energy density that can be achieved with a pulsed inductor.

1. Melting – The electrodes can be kept from melting at very high current densities using thermal mass, without the use of superconductors.
2. Containment – The very high forces generated by high current densities can be contained using inertia.
3. Losses – The losses can be held down by limiting the length of the pulse.

A simple first-order thermal and dynamic model that accounts for all of the factors in **Fig. 1** (APPENDIX D) has been used to evaluate the magnetic energy density that can be stored in an arbitrary differential element in a MES, **Fig. 2**. A summary of the results from this analysis is given in Table 1. In the top half of the table, the conductor surface is *allowed to reach melting*. The model ceases to be valid as the conductor approaches phase transition, *so* the bottom half of the table shows the case where the conductor *temperature is kept well below melting*. In this simple model, the electrodes are assumed to be made from an inner electrode layer that has optimum conductive and thermal properties, backed by a layer of lead. The thickness of the lead is chosen to limit the displacement and reaction momentum of the transmission line plates to 0.0254 cm. Since the volume of the element is the area times the thickness of lead and electrodes and the spacing between the electrodes, the energy density is weakly dependant upon the gap between the conductors. This analysis was done for the case where the conductor gap is 1 meter, wherein the energy density that can be achieved in an MES is in the range 300 J/cm^3 – 900 J/cm^3, which is

1. 10x greater than that for *superconducting* inductive energy storage. This is based upon the volume of the SC electrical windings alone – excluding the structural support, cryogens, dewars etc., &
2. 100x greater than the *best* low voltage (~6 kV) slow discharge (~1 ms) capacitors, &
3. 1000x greater than state of the art (2005) *pulsed discharge* (~100 ns), high-voltage (~100 kV) capacitor technology.

Alternatively, containment of the magnetic forces can be accomplished using the inertia of the electrodes coupled with a support structure that is the main element in limiting the displacement of the electrodes. For the 2.54 cm thick conductors without the lead backing, the pressures that the support structure would have to sustain to limit the displacement to 0.0254 cm are listed in Table 1 as $P_{STOPPING}$. It isn't clear, however, what this support structure would look like or how much it space would take up.

Concluding Remarks:

We have shown that the most practical magnetic storage mode for pulsed power is *short pulsed storage*. We have pointed out the three factors that limit how high the energy density can be in a pulsed inductor. We have demonstrated through modeling that with an electrode spacing of 1 m, pulsed magnetic energy storage can achieve energy densities in the range of 300 J/cm^3 - 900 J/cm^3 depending upon the material used for the conductors, which is much higher energy density than possible with state-of-the-art fast-discharge high-voltage capacitors. If the electrode spacing is allowed to increase indefinitely, the energy density for Tungsten limited to half the melting temperature approaches 2600 J/cc asymptotically. Finally, we have shown that the material used for the storage inductor conductors and the electrode spacing completely determines how high the energy density can be.

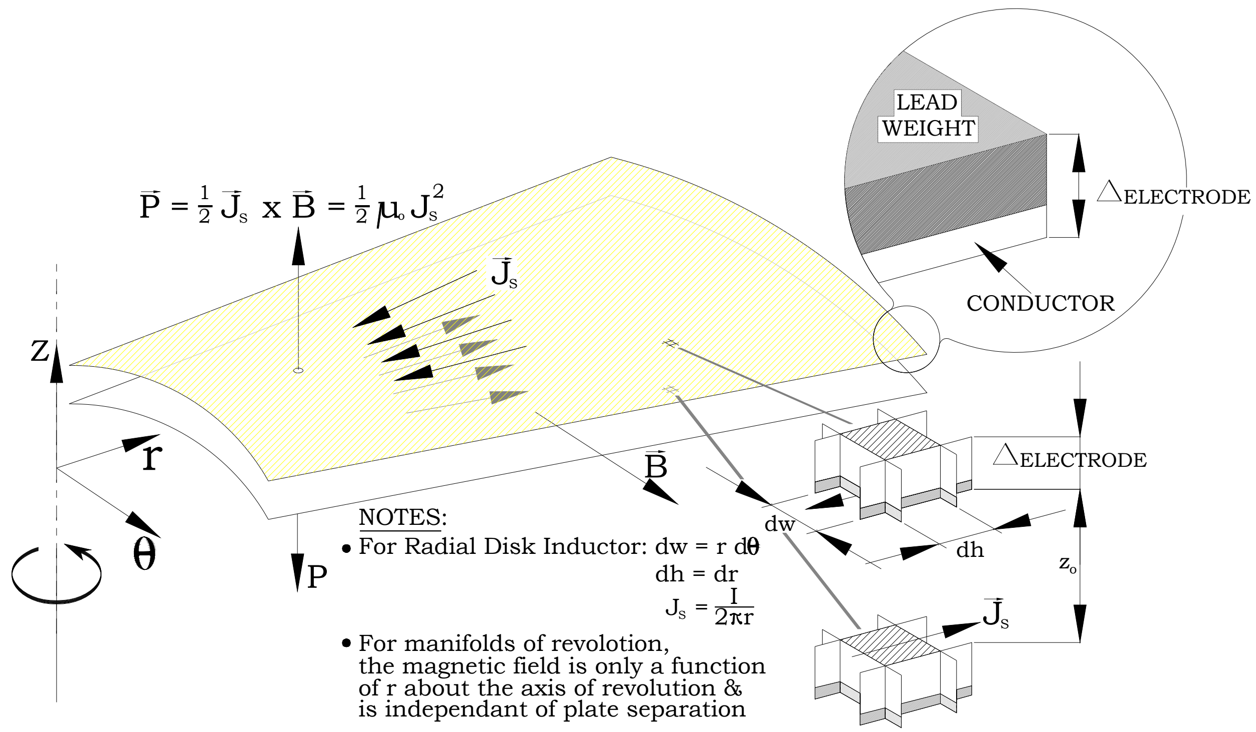

Fig. 2. A differential conductor element is used to study energy heating and dynamics of the electrodes in a MES storage inductor to determine attainable energy density.

Table 1: Achievable MES Density is solely a function of the Electrode Materials used [i].

MATERIAL	$J_{S(MAX)} = J_o$ [ii] [MA/meter]	$\mathscr{E}_{MAGNETIC}$ [iii] [J/cm³]	Q [E_{STORED}/E_{LOST}]	$\Delta_{ELECTRODE}$ [iv] [cm]	υ_{MAX} [v] [m/s]	[vi] [ksi]	T_{MAX} [°C]	T_{MELT} [°C]
Aluminum	38.3	532	5645	37	0.140	1.26	660	660
Copper	59.4	828	7112	84	0.140	2.20	1082	1082
304 SS	71.1	934	1084	120	0.140	5.04	1426	1426
Tungsten	91.0	1067	3870	194	0.140	5.63	3407	3407
Aluminum	26.6	325	5645	19	0.140	0.29	330	660
Copper	41.6	595	7112	41	0.140	0.53	541	1082
304 SS	49.9	715	1084	60	0.140	1.22	713	1426
Tungsten	64.2	889	3870	95	0.140	1.39	1704	3407

1.2 **Some Advantages of MES:**

[i] See APPENDIX D: $T_{CHARGE} = 4\mu s$, $z_o = 100$ cm, $\Delta_{ELECTRODE}$ includes 2.54 cm thick conductor with remainder lead. Transmission line back weight is chosen to limit the maximum transmission line displacement to 1 mm.

[ii] If the surface current density, J_S, is any lower the electrode won't melt at all. Melt current is essentially independent of pulse width.

[iii] Stored energy density includes the space occupied by electrodes, the electrode gap and the back weight.

[iv] The total electrode thickness includes that of the transmission line conductor (2.54 cm) and that of the lead back weight.

[v] This is the maximum velocity of the transmission line plate at the end of the pressure pulse. A consequence of limiting the maximum displacement to 1 mm is that this velocity is the same for all cases.

[vi] This is the pressure needed to stop any portion of the transmission line plate in a distance, $d_{STOP} = 0.025$ cm.

An MES Driver can be more compact than a EES Driver:
In spite of the low energy density in EES, the size of state-of-the-art EES technology for z-pinch experimentation13 is *not* determined by capacitive energy density, Table 2. The water adder/transformer sections in this design account for 69% of the 104 meter diameter while only 25% of the overall diameter represents the linear transformer drivers (LTDs) that contain the primary energy storage capacitors and switches.

An advantage of high MES energy density is that the storage inductor can be small. For comparison, the storage inductor and opening switch assembly replace everything between the primary capacitor storage and the load feed. MES makes capacitor energy density an issue,

Table 2: Energy density doesn't drive z-pinch machine size [13]

Component	Diameter Contribution [m]	Percent of Overall Diameter [%]
MITLs[vii]	6	6
Water Adder/Trans	72	69
LTDs	26	25
Tank	104	100

because the outer circumference of the storage inductor must be made large enough to accommodate connection to the low energy density capacitors. Another important advantage of MES is the intrinsic voltage gain that allows the storage capacitor voltage to be lower, possibly allowing the use of higher energy density capacitors. The outer circumference of the MES storage inductance can be made as large as it needs to be to accommodate capacitor connection without affecting the designer's ability to match the MES driver to the load. The storage inductance doesn't have to be a radial transmission line – it could be a vertical coaxial line, trading radius for height. The space gains would be negligible, however, since the inductor is so radially small to begin with due to the high energy density.

Higher Efficiencies are possible with MES by reducing the load feed inductance:
The high energy density of MES allows the more compact driver to be located closer to the load allowing the feed inductance to be significantly lower. This eliminates substantial losses due energy trapped in the feed inductance at the time of the load implosion and the lower feed inductance significantly reduces the voltage at the input to the load feed required to generate the current rate of rise required in the load.

Magnetic Parasitics are harder to Deal with Than Electric Parasitics:
Parasitics in EES are *high-energy-density* inductances whereas the drivers are *low-energy-density* capacitances. Conversely, in MES, the parasitics are *low-energy-density* capacitances and the drivers are *high-energy-density* inductances. Some of the parasitics in an MES are also inductors, but with MES the driver inductance can to be appropriately mismatched to the inductance of the feed transmission line & load to achieve *maximum* energy transfer to the load, $V_{LOAD}(t) = R_o i_{LOAD}(t) + L_{LOAD}(t)\, di_{LOAD}(t)/dt + i_{LOAD}(t)\, dL_{LOAD}(t)/dt$. It will be shown in an example that this energy transfer can be very efficient (APPENDIX H). The Isentropic Compression Experiment (ICE) driver approximates the lossless case, wherein the load is nearly

[vii] MITL stands for Magnetically Insulated Transmission Line.

entirely inductive. In this case, MES can transfer 100% of the stored energy to the load feed by matching the driver inductance to the feed inductance – this is the analog of 100% energy transfer between equal capacitors.

MES Accommodates Sustained Load Current - But Only if Desired:

The high energy density of MES introduces the option of storing a surplus of energy in the driver inductance that can be used to achieve a more sustained current in the load, if this should be desirable. This would be useful if sustained load current would produce a sufficiently more efficient fusion burn so as to more than make up for the extra initial energy. *Sustained load currents would correspond to sustained switch voltage, which would require that the design subject the switch to reduced electrical stresses.*

MES eliminates the need for Current Crossovers – Posthole Convolutes:

The high energy density of MES allows the machine to be much more compact than the EES counterpart, so the load can be fed through a single transmission line or MITL. In the case of a MITL feed, this eliminates the need for current crossover convolutes that are lossy due to the magnetic nulls that they create. This further contributes to more efficient energy delivery with MES.

Vacuum Interface should not be necessary with MES:

The vacuum interface in an EES system is a particularly significant parasitic inductance and is responsible for a large portion of the lost energy. It may be possible to eliminate the vacuum interface in an MES. In an EES driver, the voltage leads the current at the input of the MITL, so a slow geometric transition from the driver insulation to the vacuum magnetic insulation is required to minimize losses at the leading edge of the pulse. This transition in Z, called the vacuum interface, is very inductive – 13nH in the Sandia Z-machine stack and 24nH in the EES design [13]. Both POS and Ferroelectric Opening Switches (FEOS) close as the result of the arrival of a slow, thin diffusion current front at the output end of the switch that contains the entire switch current. The current at the input of the MITL *leads* [viii] the voltage because it is fully established before the voltage starts to rise due to the opening of the opening switch, so the switch is insulated behind the front before the voltage starts to rise. When a POS opens, this steep current front converts from a conduction front to a displacement front, but the electric fields are null in front of it and magnetically insulated behind it, eliminating the need for a slow geometric transition of vacuum interface. The vacuum interface represents a lot of inductance, so as with the reduced inductance of the feed transmission line, this also translates into *lower voltages* required from the MES driver to achieve a given di_{LOAD}/dt in the load and *higher efficiencies*. In Z, 20% of the originally stored energy is tied up in the vacuum-stack inductance at the time of implosion and will never make it into the radiation pulse, Table 3. There are additional losses in a vacuum stack region due to plasma crossing the electrode gap at the leading edge of the pulse when the voltage is rising up and the current is too low to provide insulation. In MES these losses are eliminated because the maximum current is already fully established at the output end of the opening switch and leaves the switch as an already fully insulated displacement current wave into the MITL.

[viii] It is a common misconception that the "voltage leads the current in an inductor", in our case the load feed. In fact, the change in voltage leads the change in current in an inductor. In a lossless inductor with steady current flowing in it and zero voltage on it, the current doesn't begin to change until the voltage changes to non-zero.

Table 3. MES may eliminate the vacuum interface, improving efficiency & reducing voltages. Format: Energy MJ/%

Location	Z	Petawatt Example [13]
Initial Store	12 MJ/100%	182 MJ/100%
Arrives at Stack	3.3 MJ/28%	88 MJ/48%
Lost in Stack	2.3 MJ/20%	71 MJ/39%

MES drivers can have load current rise times an order-of-magnitude faster than EES with conventional opening switches:

Voltage gain and lower feed inductances make MES rise times much faster than EES rise times. The MES load current rise time with a conventional opening switch is limited by both the load/feed inductance and the parasitic capacitance at the input to the load feed, **Fig. 3**. Both the load/feed inductance and the parasitic capacitance at the input to the feed, however, can be made very small making it possible to achieve load current rise times that are an order of magnitude faster than possible with EES.

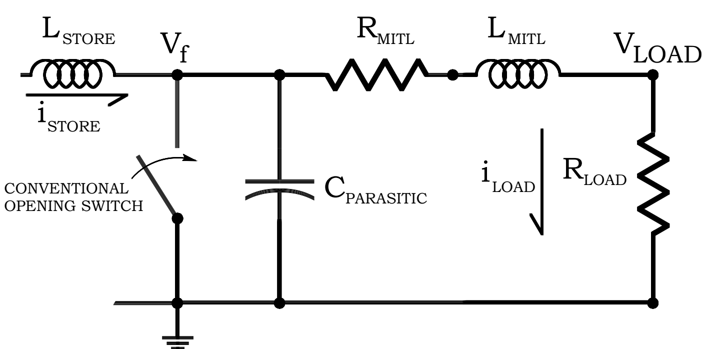

$$di_{LOAD}/dt = \frac{1}{L_{LOAD}C_{PARASITIC}} \int (i_{STORE} - i_{LOAD})dt$$

Fig. 3. In a conventional MES, the storage current has to charge the small parasitic capacitance before the voltage on the feed transmission line/LOAD can rise up to drive Ldi_{LOAD}/dt.

There is no substantial voltage accept for during the instant that energy is delivered to the load:

The opening switch provides voltage gain, allowing the entire system to operate at voltages much lower than the load voltage, allowing most of the driver to be more compact. Only the voltage on the switch and the load goes high for a few tens of nanoseconds during the time that energy is being delivered to the load. The extremely short duration that the voltage is high makes it possible to achieve extraordinarily high electrical strengths in all of the electrically stressed elements in the output.

1.3 <u>High grade ferroelectrics could be used to make a pulsed power class opening switch</u>:

Future needs for larger currents, faster rise times, and current shaping create a need for simpler, more compact, cost-effective, controllable, pulsed power grade opening switches. This need could be addressed by further research and improvement in state-of-the-art MCPOS. New technologies such as Ferroelectric Opening Switches (FEOS) also have the potential for meeting this need, but higher performance materials than those demonstrated so far[14, 15, 16] would have to be used to make an opening switch that would be suitable for pulsed power. FEOS on-state impedances are low compared to those of fusion and ICE loads, preventing a substantial pre-pulse current foot. Solid-state FEOS construction provides high-reliability and offers the advantage of fewer support systems such as gas supplies, regulators, extra cabling and plumbing needed for triggered spark-gaps. High solid electrical breakdown strengths, large electronic dipole moments, low saturated permittivity's and high domain densities in solid-state Perovskites make compact, high charge capacity switches possible.

Conditions are favorable for Magnetic Flashover Inhibition (MFI) at the output of the FEOS:

The current in the FEOS propagates through the switch as a relatively abrupt displacement front that contains the entire switch current. The electric and magnetic fields are zero in front of the current front and fully established behind it. The FEOS opens when the concentrated displacement front arrives at the output face of the switch, r = b, **Fig. 4**. When the FEOS opens, the displacement front breaks out into the vacuum MITL and continues as a vacuum displacement current front. Physics dictates that the current cannot change instantaneously, so the current in the vacuum front must match that on the output face of the FEOS just before it opened. The current in the displacement front actually *leads* the voltage behind it, because the current is already fully developed before the voltage starts to rise due to the opening of the switch, so the region behind the displacement is fully magnetically insulated. At the output end of the FEOS, the Poynting vector points away from the switch face so that MFI condition is met. Our plan is to construct a wave model to verify these arguments and show that the necessary conditions for Magnetic Flashover Inhibition (MFI) exist behind the displacement front17.

On the input side of the switch the Poynting Vector is directed toward the switch **Fig. 3**, so MFI doesn't apply. Inductance on this face is not an issue, so it can easily be insulated using conventional methods such as long distances and oil.

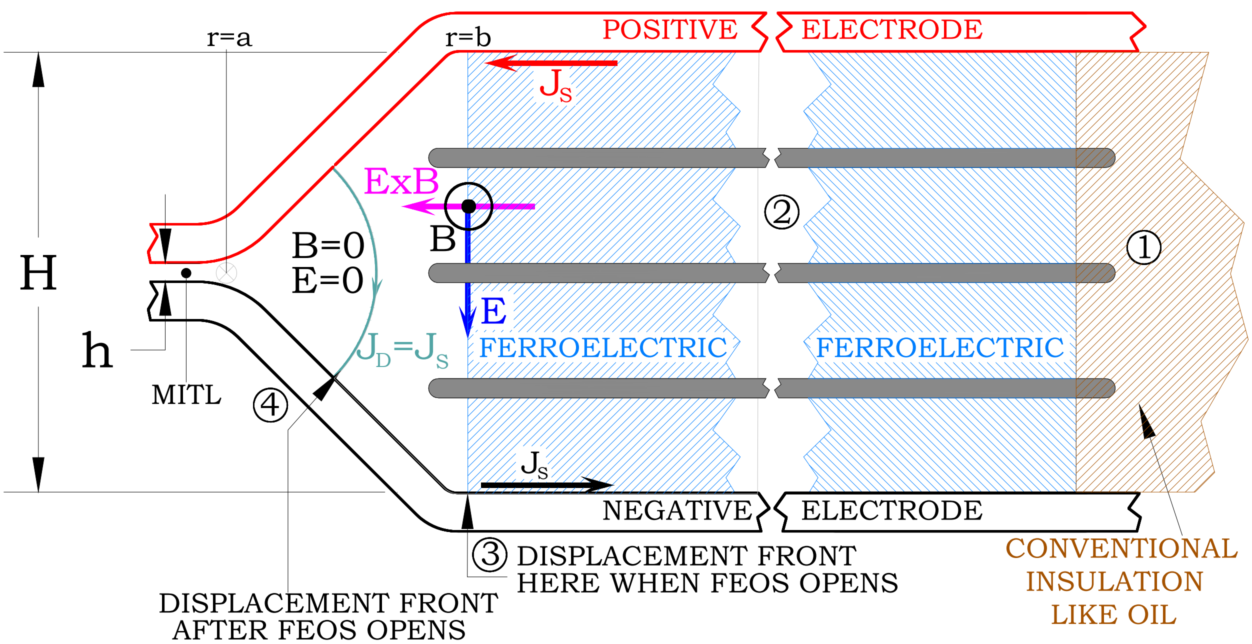

(b)

Fig. 4. Profile of FEOS in 60MA driver, (b) Current waveforms for 60MA driver

FEOS Traps Magnetic Energy:

An FEOS switch naturally traps magnetic energy in the MITL/LOAD loop because it can conduct freely in the reverse direction after it opens in the forward direction.

FEOS Scales Well:
FEOS is very suited for scaling to larger machines due to a natural ability to integrate in parallel. When one parallel connected switch starts to open it shunts current to others and speeds up their switching.

High Current Density:
Ferroelectric switches are displacement current devices, so they can sustain current densities that are orders of magnitude higher than conduction mode solid-state switches. The known switching losses[18] are so low that there is essentially no limit on current density into ferroelectrics. require them to switch at close to 1 GHz for sustained times.

Fast Switching:
The dipole moment in a Perovskite unit cell change from one polarization to the opposite on a picosecond time frame. Domain walls travel at less than the speed of sound as dipoles on the

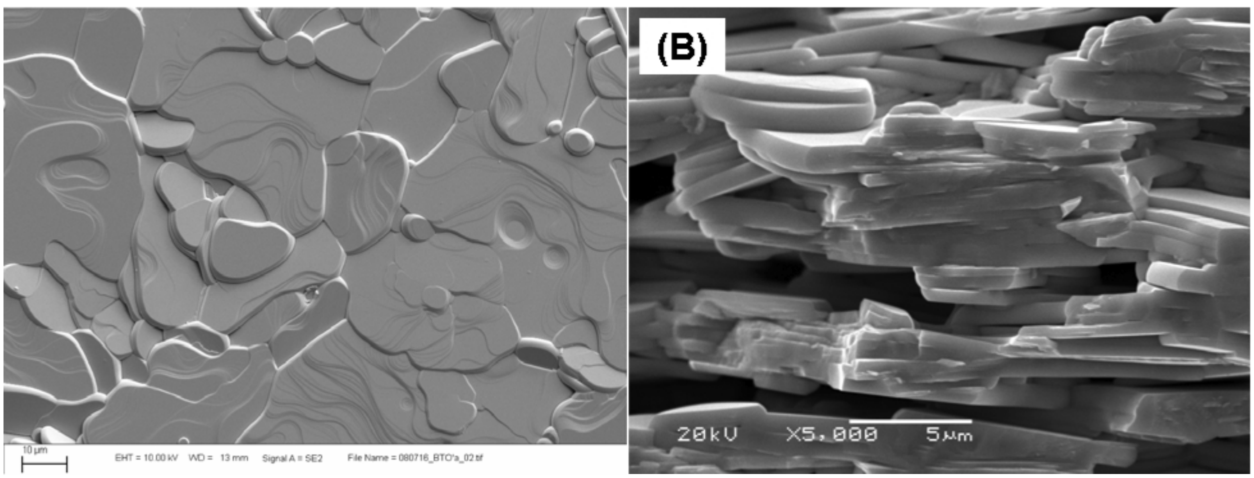

(a) (b)

Fig. 5. Grains can be seen in a BTO ferroelectric made in the lab at Sandia. (a) plan view, (b) cross sectional view. Crevices are where material fell out when the wafer was broken.

boundaries flip polarization. Points throughout the volume where dipoles begin flipping from the originally poled state to the opposite form new domains. In polycrystalline ferroelectrics this domain nucleation occurs at *every* grain boundary. The grains can be seen in Scanning Electron Micrographs (SEMs) of a typical polycrystalline ferroelectric in a plan view in **Fig. 5**(a) and in a cross sectional view in **Fig. 5**(b). The domains are nominally <20 um across in the plan view and thinner in the cross sectional view. Data reported19 for Lead Zirconium Titanate (PZT) with an electrical stress of 20 kV/cm indicates a speed of sound of ~4300 m/s. Simulations have been reported20 that indicate domain wall velocities of ~2000 m/s at an electric stress of ~750 kV/cm in Barium Titanate ($BaTiO_3$). Therefore, we roughly estimate that the walls of these growing domains can close on each other in,

$$t_{CLOSE} < 10 \text{ um}/2000 \text{ m/s} = 10 \text{ ns}$$

We conclude that operating in the conventional mode; a ferroelectric opening switch volume should be able to transition from one polarization to the opposite polarization in less than 10 ns, depending upon the material and the applied electric stress. This sets a lower limit on the time that the storage inductor can be charged with current in a MES application. Our experiments show that a PZT ferroelectric volume of 2.5 cm diameter x 0.16 cm thick acts like an electrical short for storage inductor charging times of <200 ns in a MES circuit. By contrast, switching occurs in the time that it takes the ferroelectric to transition from the high-permittivity state to the low-permittivity state, that is to go around the corner on the P-E loop. Depending upon the current density being applied to the ferroelectric during the charging phase, this time should be much faster than the time it takes for the whole ferroelectric volume to transition from one polarization to the other (<<10 ns). In fact, switching experiments have been conducted wherein the load current rise time was less than 10 ns and this was circuit limited.

Potentially High Dielectric Strength:
The ferroelectric materials that are being considered were developed for optical applications, so they are either a pure single crystal or a multi-crystalline slab that has been compressed under heat into optically pure substrate. In contrast to conventional solid insulators, like Mylar, optical purity guarantees an extremely low flaw density, which we envision may yield nearly the same electrical strengths in thick samples as have been obtained in thin samples, 8MV/cm, 50 ns, ~100 - 200 nm thick.

The applications that are most suited to the ferroelectric MES are characterized by load pulse durations of only a few tens of nanoseconds. Even polycrystalline ferroelectrics have been experimentally shown to exhibit extraordinarily high electrical strength (>1 MV/cm) when the voltage on the switch is this short in duration. Experiments have demonstrated that the MES driver circuit can be matched to the load so that after the short pulse there is very little left over energy or ringing that could cause electrical breakdown of the switch.

Practical issues will make it necessary to construct large area switches from many ferroelectric tiles joined at the edges with epoxy. Epoxies also exhibit extraordinarily high electrical strengths (> 1MV/cm) when electrical stress duration is limited to a few tens of nanoseconds. In conclusion, both the ferroelectrics and the filler materials used to join them will exhibit unprecedented electrical stress performance under the operating conditions made possible with this technology enabling a very large area switch to be constructed from many smaller tiles.

MES with FEOS Delivers Current Gain:
In addition to providing voltage gain from the charge voltage to the load voltage, FEOS *exclusively* provides <u>*current gain*</u> from the storage inductor current to the load current, **Fig. 5**(b). The extra charge needed for current gain comes from the capacitance of FEOS.

2.0 Experimental results

2.0 Demonstration of $BaTiO_3$ as an opening switch

Korea Electrotechnology Research Institute [14, 15] (KERI) used a Murata DE1207F103Z2K capacitor as an opening switch to generate nominal 150 ns rise time, 10 kV voltage pulse into a 1 kohm load resistor. *The goal of this experiment is to reproduce the KERI result using the closest available comparable capacitor, Murata DEBF33D103ZAB.* It is surprising that these $BaTiO_3$ capacitors can be used effectively as an opening switch since they exhibit a very rounded P-E loop, Fig. 6.

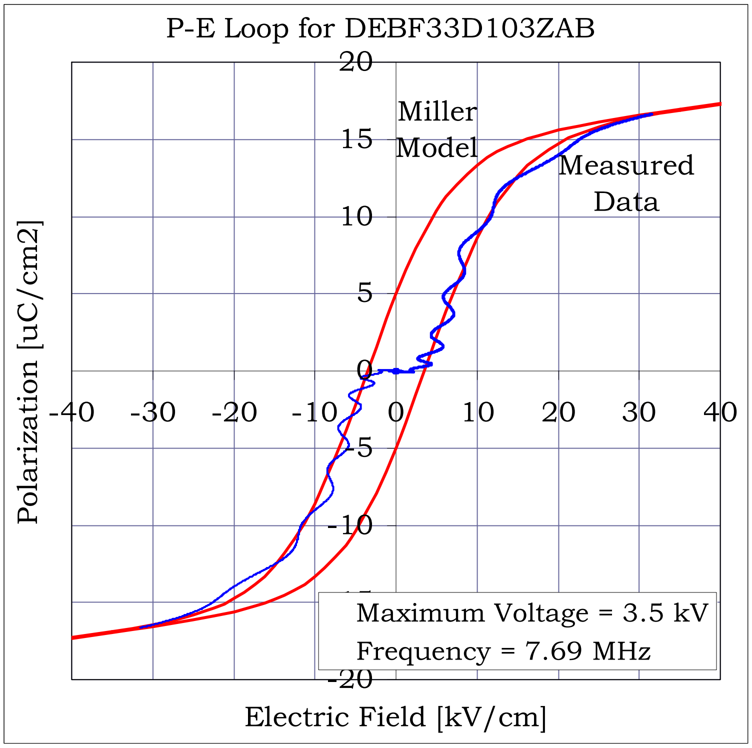

Fig. 6. The measured P-E Loop gave us the values for the material parameters.

The P-E loop was generated by opening the spark gap wide enough so that it would never close – di/dt is finite due to the rounded corners of the P-E loop. Polarization is the integrated current into the FEOS divided by the area of the FEOS. Electric field is the voltage on the FEOS divided by the thickness of the wafer. The P-E loop in Fig. 6 is a plot of the measured polarization versus the measured electric field. The ripple in the measured P-E loop is due to secondary ringing that seems to be on all of our data. This ringing occurs in direct correspondence with the fast rise time. When the circuit is modified to spoil the rise time, the secondary ringing disappears. The material parameters in the Miller Model [22] were adjusted to obtain a best fit to the measured P-E loop and the resultant values were used in our pulser circuit simulation, Table 4. It is critical that the P-E loop be measured under the same conditions that it will be operating under in the pulser circuit particularly the same frequency. The other circuit parameters were obtained by shorting out the FEOS and ringing the circuit.

Table 4. Experimental & Model parameters used in the comparison.				
		Model	Experiment	Comments
FEOS Switch:				
$e_{r(SAT)}$		400	--	
P_s	μC/cm²	14.50	--	spontaneous polarization
P_r	μC/cm²	5.00	--	remnant polarization
E_c	kV/cm	3.70	--	coercive field
d	kV/cm	5.15	--	
D_{WAFER}	cm	1.00	1.00	wafer diameter
N_{WAFERS}		9	9	number of parallel wafers
A_{WAFER}	cm^2	7.07	7.07	total wafer area
$d_{THICKNESS}$	cm	0.10	0.10	wafer thickness
Circuit Components:				
V_o	kV	5.5	5.50	initial charge voltage on C_o
C_o	uF	0.080	0.080	storage capacitor
R_{STORE} [ix]	ohms	6.745	2.045	series resistance in RLC loop
L_{STORE}	uHy	0.244	0.244	energy storage capacitor
$V_{SPARK-GAP}$ [x]	kV	3.04	0.76	spark gap break over voltage
L_{LOAD}	uHy	0.11	0.11	load inductance
R_{LOAD}	ohms	33.00	33.00	load resistance

Our experimental set up is shown in **Fig. 7**. In order to get a good fit between the simulated and measured L_{STORE} charging currents, **Fig. 8**(a), it was necessary to add 6.5 ohms to R_{STORE} in the model. This added resistance also made the amplitudes of the measured and simulated load currents and voltages match, **Fig. 8**(b). It isn't clear what the source of this resistance is, but we suspect that the arc resistance of the "Slapper Switch", **Fig. 7**, may have increased when the storage loop current, I_{STORE}, was reduced by the addition of the FEOS. The original value of R_{STORE} was obtained by placing a short in place of the FEOS, so the addition of the FEOS would tend to reduce the current in the slapper switch and increase the arc resistance. In order to get a good match to the pre-foot on the load current and voltage, it was necessary to open up the load

[ix] Resistance was increased by 6.5 ohms over the value measured in the ringing
[x] Gap closing voltage had to be increased by 1.5 kV in the model to make it better

spark gap by 30 mils in the simulation over the 10 mils used in the experiment, **Fig. 7**. The 0% to 100% rise time of the load waveforms is less than 10 ns. These kinds of rise times are possible with this technology because it is the low energy density of the capacitance at the switch output that limits the rise time, whereas with voltage driven technology, the high energy density of the inductance at the last switch output limits rise time in the load.

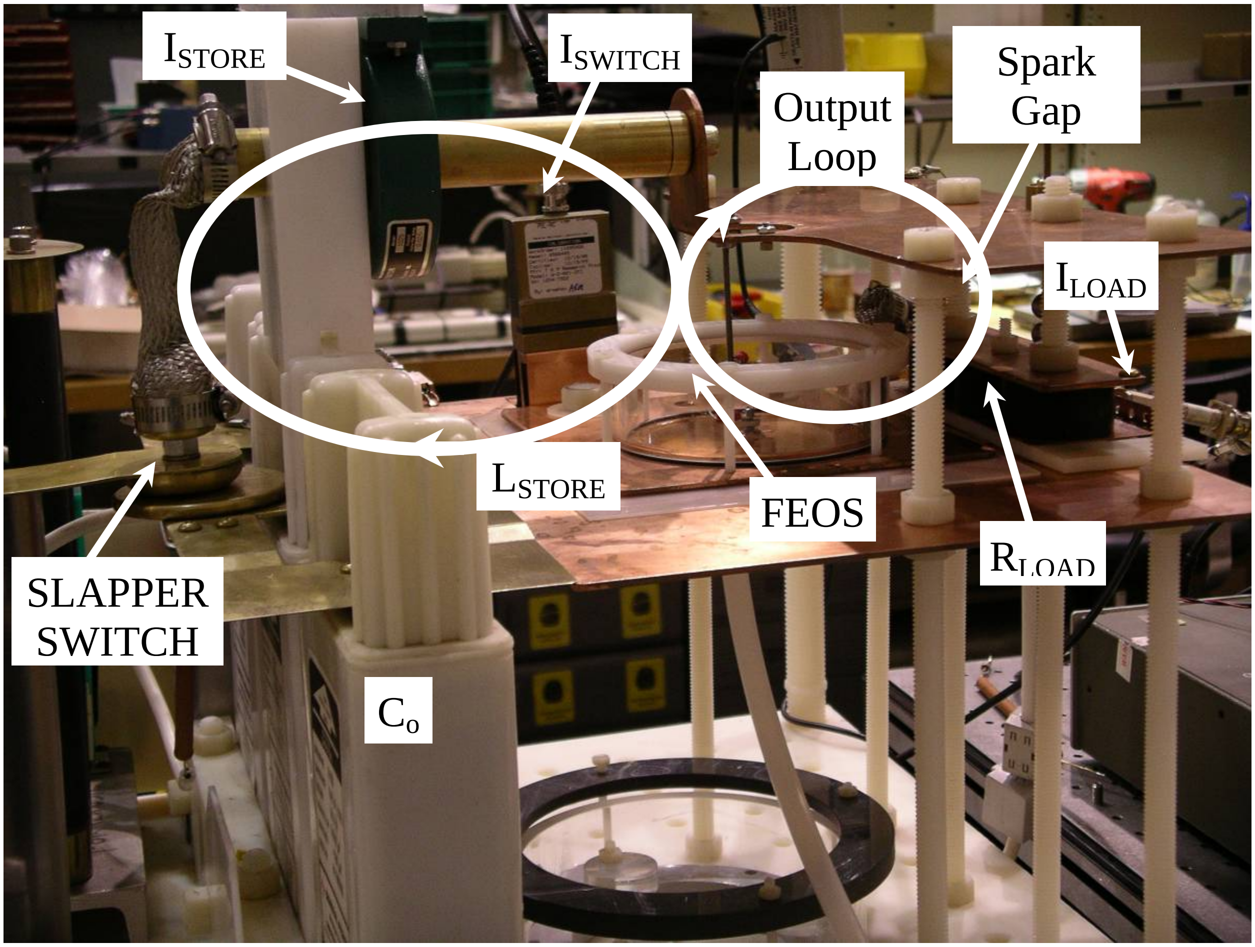

Fig. 7. Our experimental set up can be used to generate P-E loops and pulses into a load.

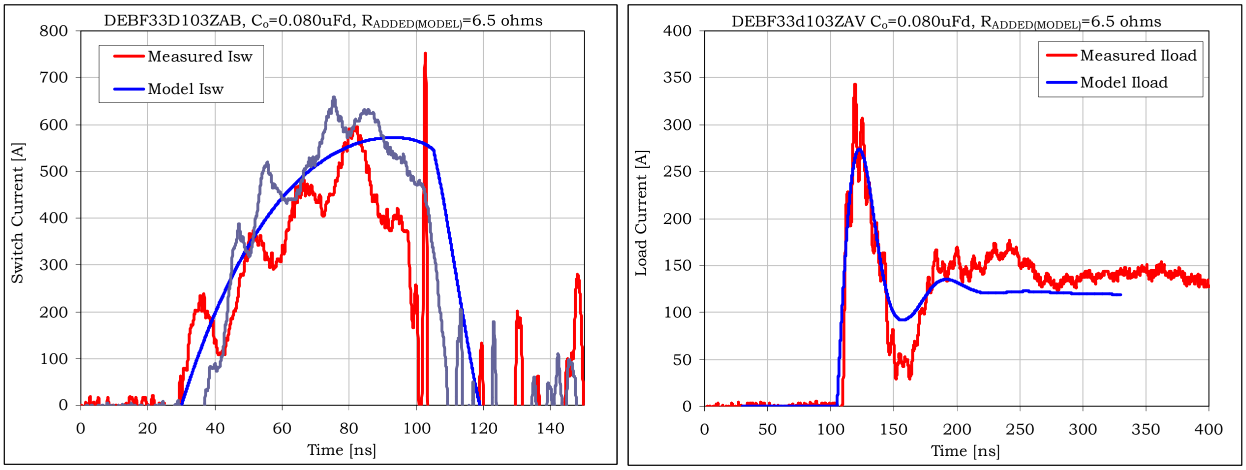

(a) (b)

Fig. 8. The addition of a 6.5 ohm resistor in the storage loop made the charging and load (b) currents in the simulation and experiment match pretty well.

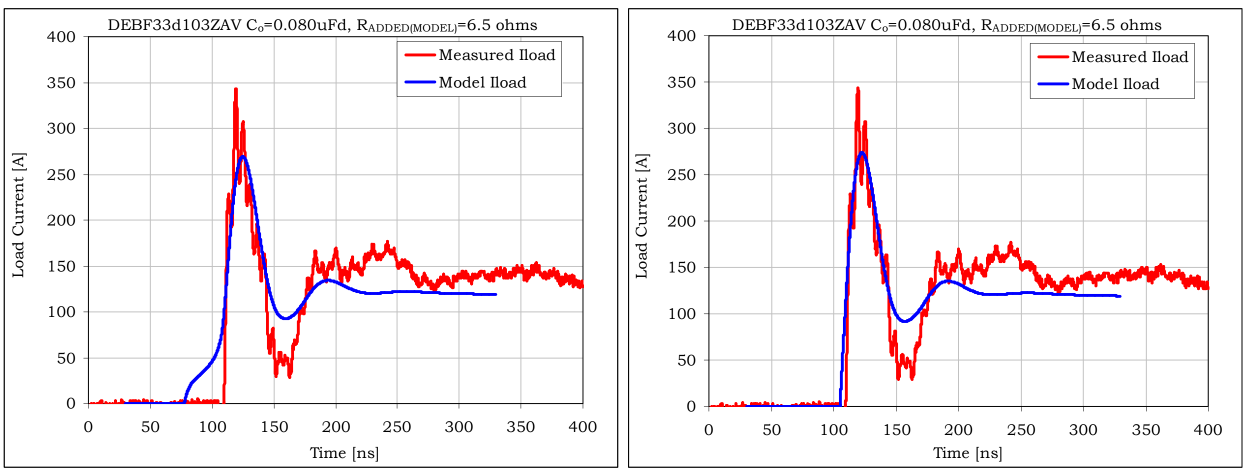

(a) (b)

Fig. 9. The spark-gap setting mainly affects the pre-foot on the load waveforms. (a) Spark-gap set at 40 mils (MODEL ONLY), (b) Spark-gap set at 10 mils (MODEL ONLY).

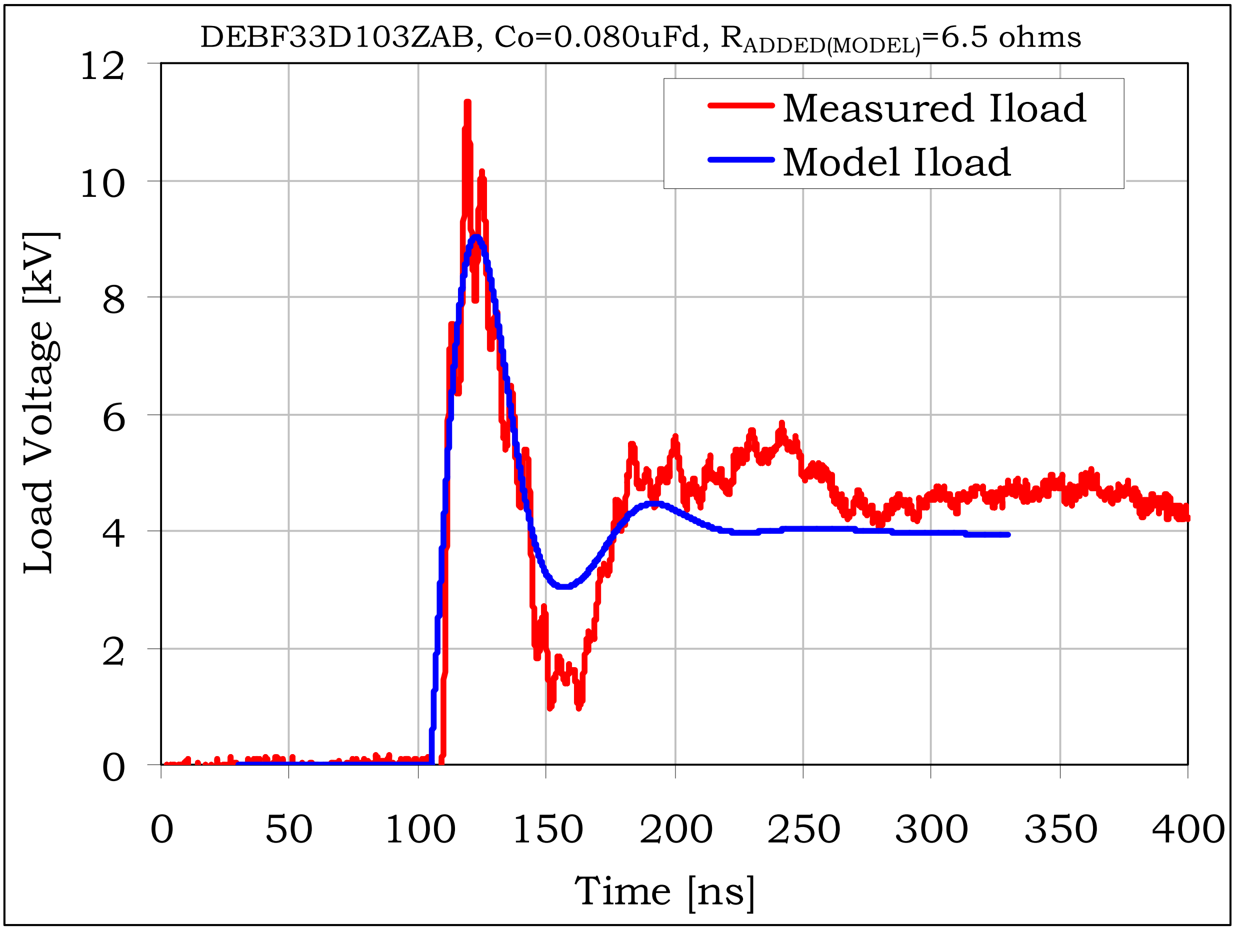

Fig. 10. The load voltage rises to 9 kV corresponding to 3.9 MW peak power (Shot 19).

The load resistor is 33 ohms, so the load voltage rose to about 9 kV, corresponding to a peak power into the load of 3.9 Mega Watts, **Fig. 10**. Voltage gain is a feature of this technology that doesn't occur naturally with voltage driven technology, that is, without a transformer, MARX, etc. The initial charge voltage on C_o was 5.5 kV, demonstrating a voltage gain of 1.6X. The voltage gain is relatively small for this material since the P-E loop is so skewed and rounded. Voltage gains of more than an order of magnitude higher than this are possible with better ferroelectric materials. The switch that delivered this power to the load with 10 ns 100% rise time consisted of a 1 cm diameter and 1 mm thick wafer, smaller than a dime, **Fig. 11**. Studies conducted with our simulation have shown us that the energy transfer from the initial store to the load can be optimized by properly matching the area of the switch to the resistance of the load.

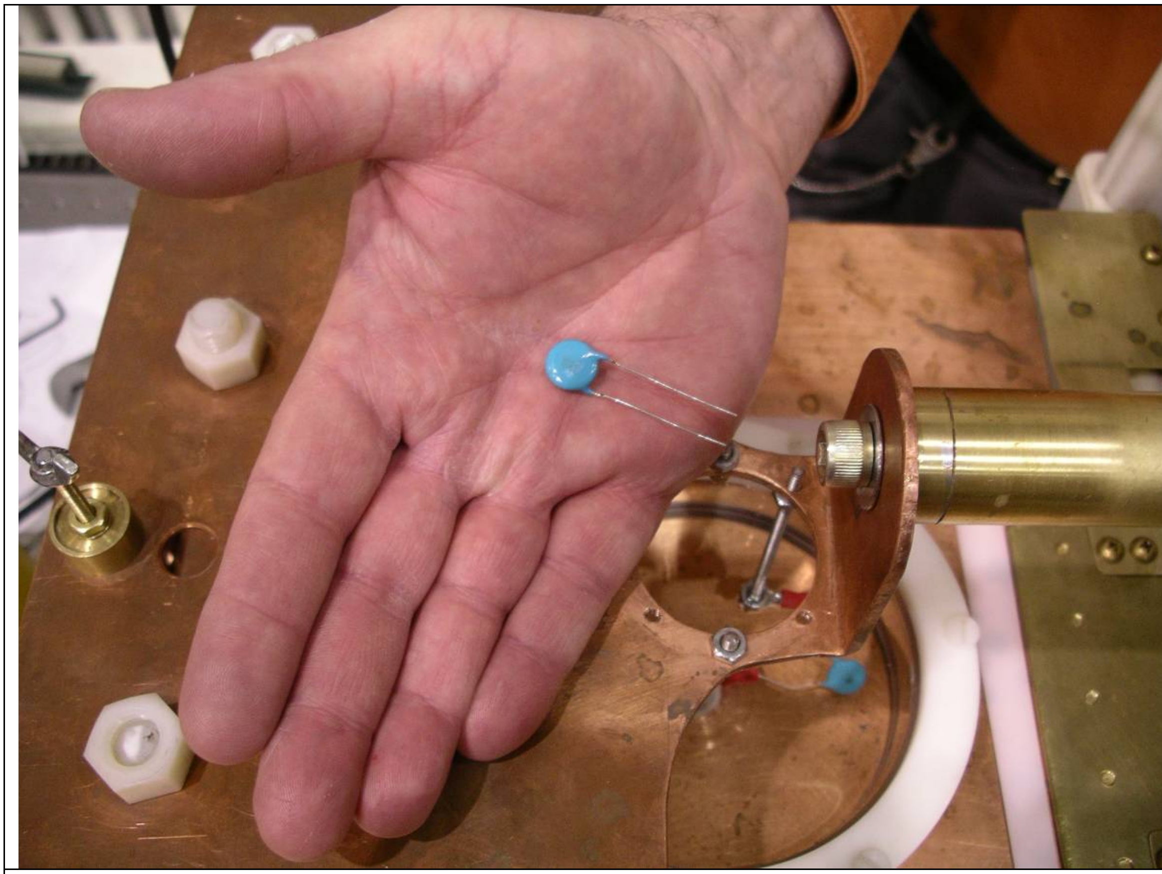

Fig. 11. The ferroelectric opening

3.0 Conclusions:

We have demonstrated that the ferroelectric switch concept works. Even with a material that we consider to highly suboptimal, a switch the size of a dime was able to hold off 9 kV and deliver 250 A to a 33 ohm load with a 0% to 100% rise time of 10 ns. We find this performance encouraging, but believe that a material with a taller and more squared off P-E loop, such as single crystal lithium tantalite would yield significant performance gains, Fig. 12. A squared off P-E loop has a bigger impedance contrast between the on state and off state with the on state looking essentially like a short circuit. A taller P-E loop allows the switch to smaller for the same current and conduction time. Experiments with single crystal lithium tantalite revealed that it wouldn't initiate dense volumetric nucleation when subjected to an electrical stress many times the coercive field.

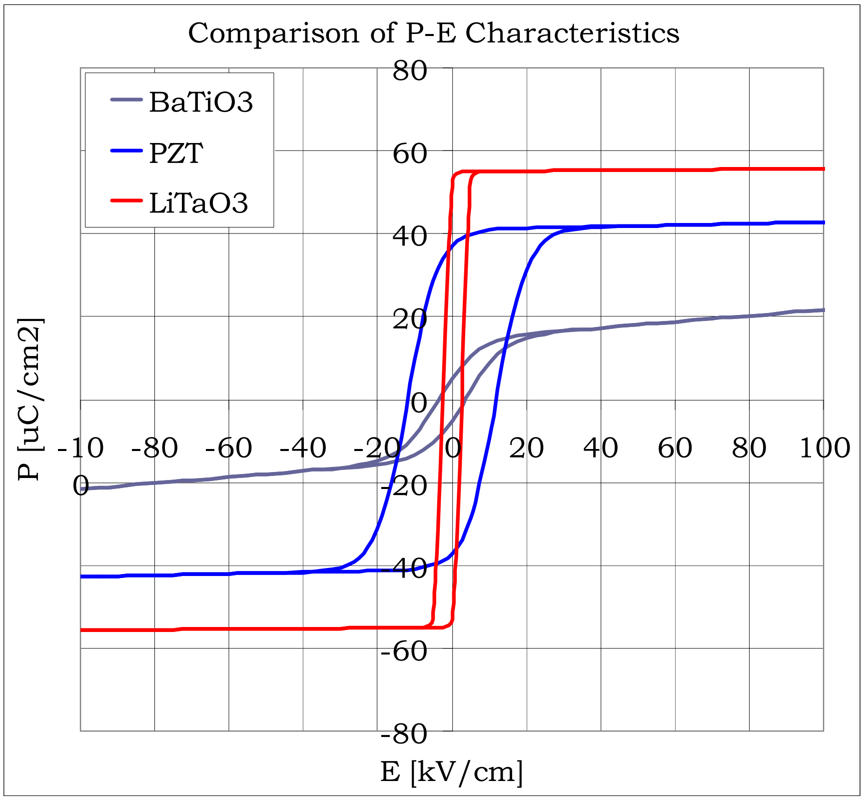

Fig. 12. A more squared of P-E loop should yield performance gains.

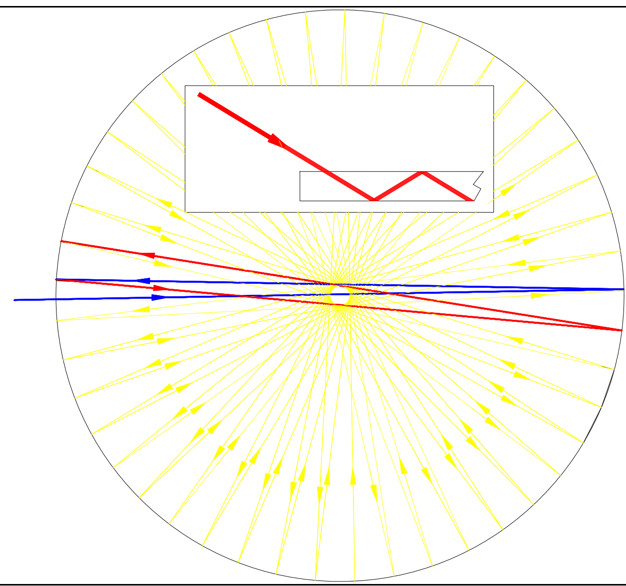

Fig. 13. We plan to introduce a laser beam into the edge of the single crystal wafer an allow it to bounce through out the volume in the wave guide formed by the two crystal faces.

The result is that the switch would never conduct in the first place, preventing the storage inductor from being charged with energy. We tried roughing up the surface of the material before vapor depositing the electrodes, but this didn't solve the problem.

Our goal is therefore to discover a way to induce volumetric domain nucleation in the higher quality materials such as $LiTaO_3$ and achieve an opening switch that will impact the future of pulsed power. Two approaches should be investigated. Since it is believed that grain boundaries are needed to initiate dense nucleation, multi-crystalline lithium tantalite could be synthesized to promote nucleation. A second approach is based upon the fact that in the field of optics, lasers are used to pole high quality single crystal ferroelectrics, including lithium tantalite. It may be possible to induce switching by electrically stressing the crystal at many times the coercive field and then introducing a pulsed laser beam. The laser would be of appropriate wavelength and intensity and directed into the edge of the wafer to allow it to bounce around in an orderly manner in the wave guide formed by the two crystal surfaces, Fig. 13. Since this will illuminate the entire volume of the crystal at the speed of light, it may be able to initiate dense volumetric nucleation.

Ferroelectrics may represent an entirely new class of high voltage, high current switch materials. Continued research is highly recommended

APPENDIX A: Determination of the correct skin depth for a sine current that is turned on at t=0.

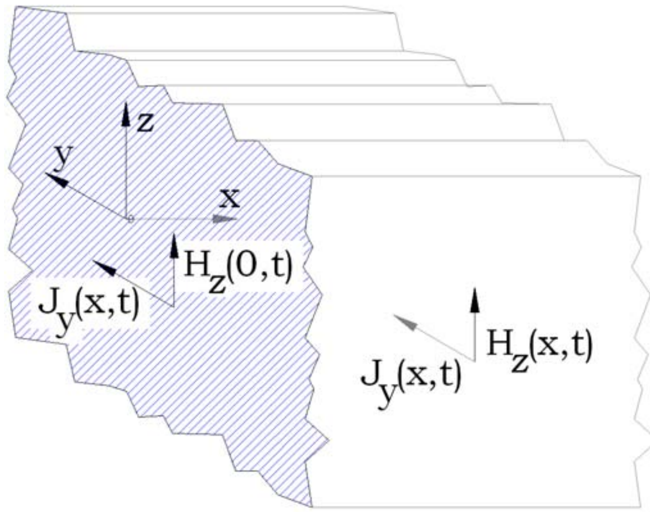

Fig. A1. Semi-infinite plane for current diffusion calculation.

Consider application of a magnetic field, Hz(0,t), that yields a current density, $J_y(0,x)$, Fig. A1,

$$J_y(0,t) = J_o\, u(t)\sin[2\pi t/T] \quad \text{[amperes/width]} \tag{A.1}$$

where, T = the temporal period of the sinusoid
J_o = the amplitude of the current density on the surface of the conductor

$$u(t) = \begin{cases} 0, & t < 0 \\ 1, & t > 0 \end{cases} \tag{A.2}$$

to a semi-infinite slab of conductor. The current density as a function of time and space is given by Knoepfel21 as,

$$J_y(x,t) = \underbrace{\boxed{J_o e^{-x/\delta}\sin(2\pi t/T - x/\delta)}}_{\text{Steady State}} - (2/\pi^{1/2})\, J_o \int_0^{\lambda_o} \sin\{2\pi t/T - ½[(x/d)/\lambda]^2\}\, \exp(-\lambda^2)\, d\lambda \tag{A.3}$$

where, $t \geq 0$
$\delta = [T/(\pi\sigma\mu)]^{1/2}$
$\lambda_o = ½\, \delta\, (x/\delta)/[\{t/(\sigma\mu)\}^{1/2}]$

NOTE: current and magnetic fields obey the same diffusion equation see Knoepfel, page 47. Therefore you can replace J_y everywhere with H_x

The first half of this equation is the solution for the application of a steady-state current density,

$$J_y(0,t) = J_o \sin[2\pi t/T), \tag{A.4}$$

to the conductor surface, so it is the term for which the skin-depth applies,

$$\delta = [T/(\pi\sigma\mu)]^{1/2}. \tag{A.5}$$

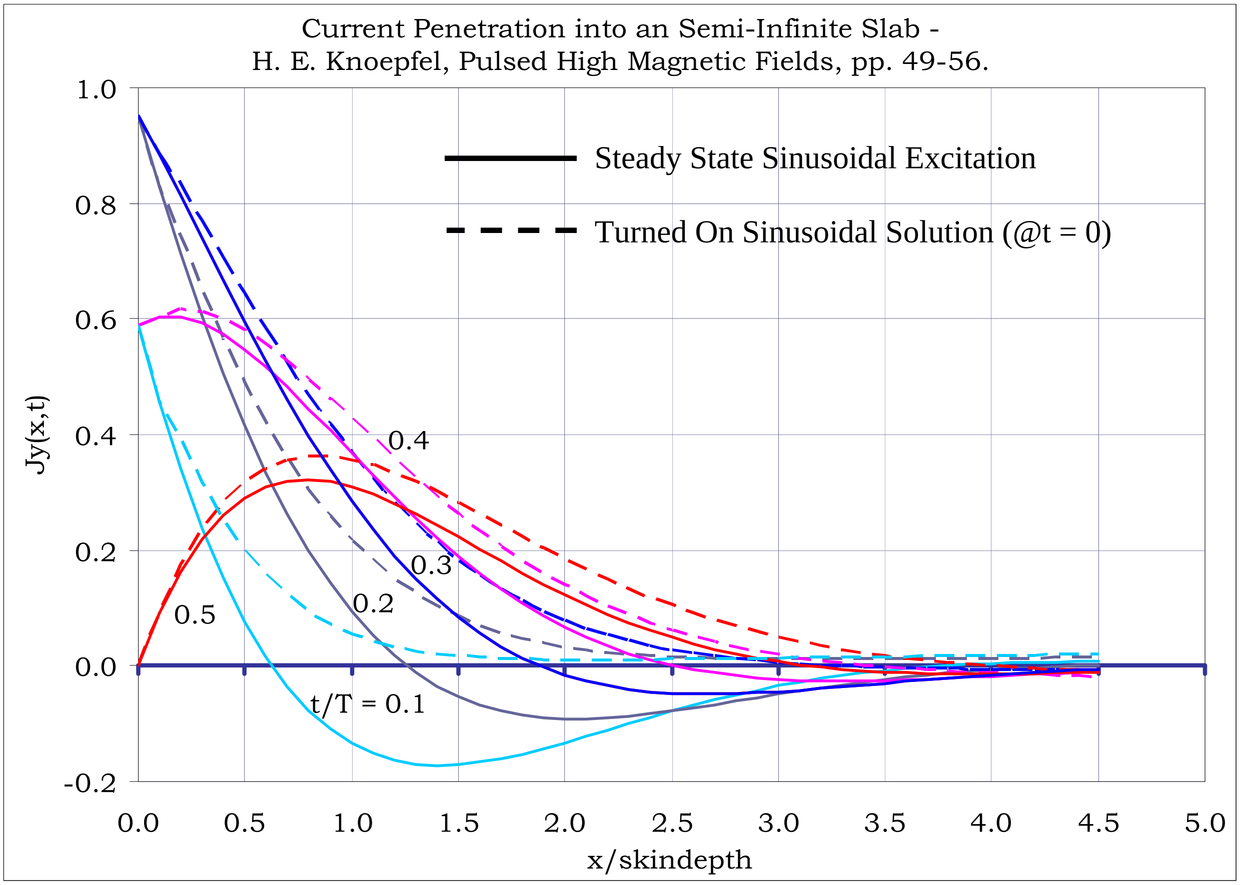

Fig. A2. Current density as a function of time and depth in a semi-infinite conductive slab.

The transient solution (A.3) is plotted along with the steady-state solution in Fig. A2.
The justification for using the steady-state form of the skin depth, is that for all times in the range, $0 < t < ½T$, the current density that results from turning the surface sinusoidal excitation on at $t = 0$, penetrates deeper where it is non-zero than the current density that results from the steady-state excitation. The negative lobe on the steady-state solution is due to the negative current from the previous half-cycle reversing out of the conductor. We conclude that the penetration of the transient current is deeper than that of the steady-state currents so it would be worst case if we use the steady-state skin depth for the transient calculations. We will use this form of the skin-depth with T replaced by 4xt, where t is the time of the differential calculation. By doing this we are treating the current at any given moment as though it is the first quarter cycle of a turned on sinusoid, better representing the progressive penetration of the current into the conductor with time. At the end of the charge cycle when $t = T_{CHARGE}$, then we are using the full skin-depth for the actual charging waveform.

APPENDIX B: Parameters used in the Dynamic & Thermal Calculations.

Table B1. Coefficients for calculating conductivity versus temperature

Material	ζ	ξ
Aluminum	1.64	0.00429
Copper	1.03	0.0068
304 Stainless	1.00	0.00651
Tungsten	1.00	0.0045

Table B2. Coefficient of Linear Expansion

Material	β [$^{o}C^{-1}$]
Aluminum	2.52E-05
Copper	1.66E-05
304 Stainless	1.73E-05
Tungsten	4.50E-06

Table B3. Other Material Parameters Used in the Model.

Material	Density [kg/m^3]	Specific Heat [J/Kg-K]	Thermal Conductivity [W/m-K]	Electrical Conductivity [ohms-m]$^{-1}$	Melting Temperature [^{o}C]	Acoustic Velocity [m/s]
Aluminum	2700	870	202	3.77E+07	660	6400
Copper	8960	381	387	5.98E+07	1082	4800
304 Stainless	8020	460	14	1.39E+06	1426	4500
Tungsten	19300	130	174	1.77E+07	3407	5250

APPENDIX C: An Isentropic Compression Experiment Driver Design

Another example of an effective application of Magnetic Energy Storage with an FEOS is the compact ICE driver presented here. Different materials and different Equation of State studies require a variety of drive current waveforms, Fig. C1. The optimum load current waveform depends upon the material that is being studied. It isn't possible to exactly match all of these waveforms using an EES driver that combines the inputs of a large number of RLC modules in parallel, Fig. C2 & C3, but MES matches the required current with ease.

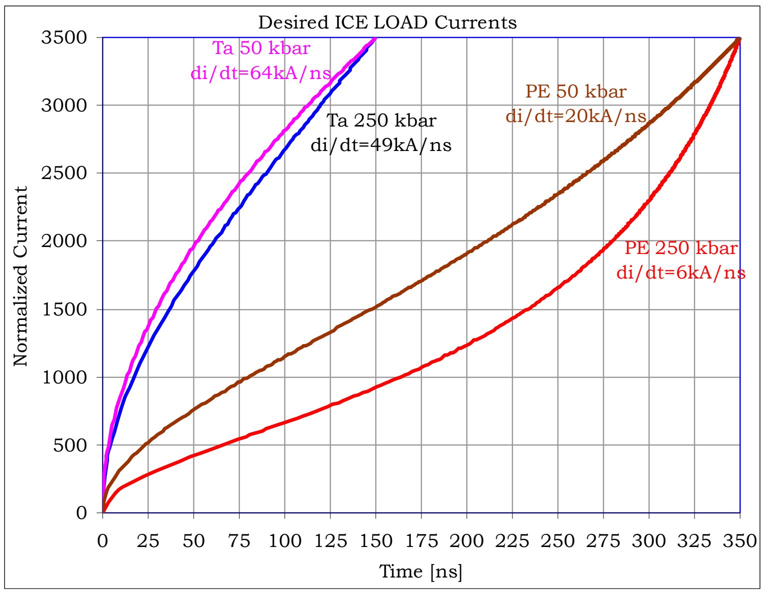

Fig. C1. There are a variety of load current waveforms that the Equation of State folks need.

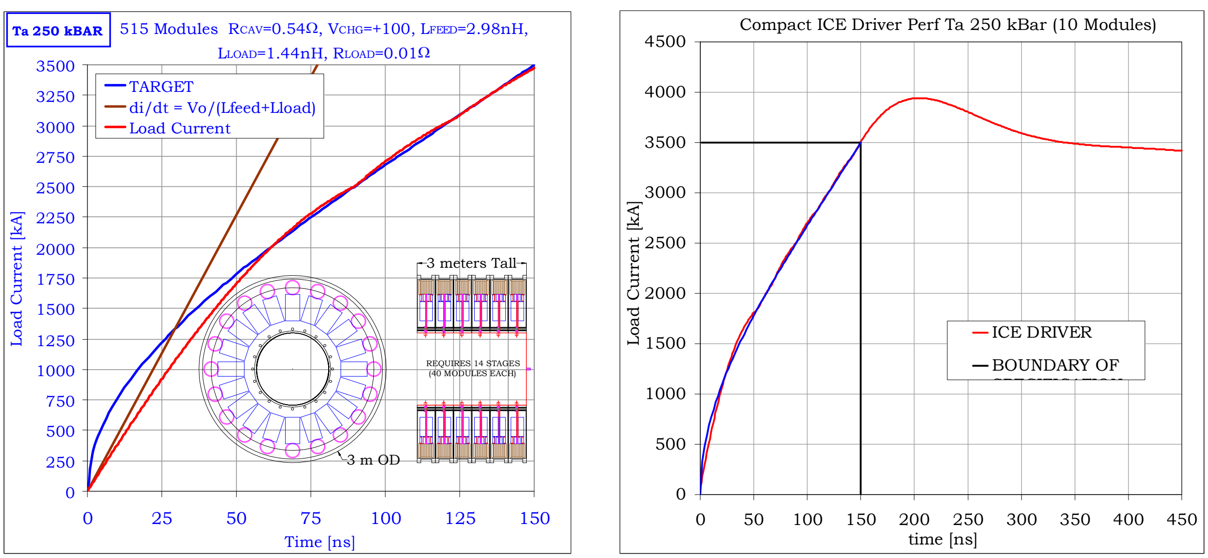

(a) (b)

Fig. C2. (a) EES is limited to a maximum slope of $V_o/(L_{FEED}+L_{LOAD})$ so it can't match the current waveform for Ta 250 kBAR.

(b) MES easily fits Ta 250 kBAR as well as Ta 50 kBAR with only 10 modules.

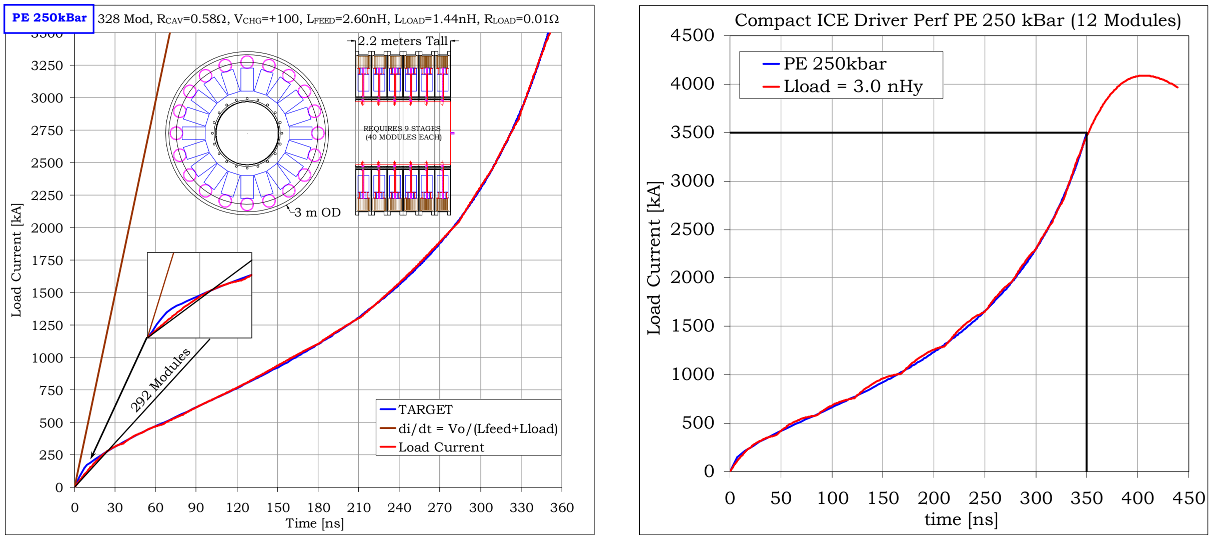

(a) (b)

Fig. C3. (a) EES is limited to a maximum slope of $V_o/(L_{FEED}+L_{LOAD})$ so it can't match the current waveform for PE 250 kBAR at the beginning.

(b) MES easily fits PE 250 kBAR with only 12 modules, even with 10 nHy load inductance (not shown).

The circuit model for the MES driver that was used to generate the results above is shown in Fig. C4. The conceptual MES hardware that would achieve this performance is shown in Fig. C5.

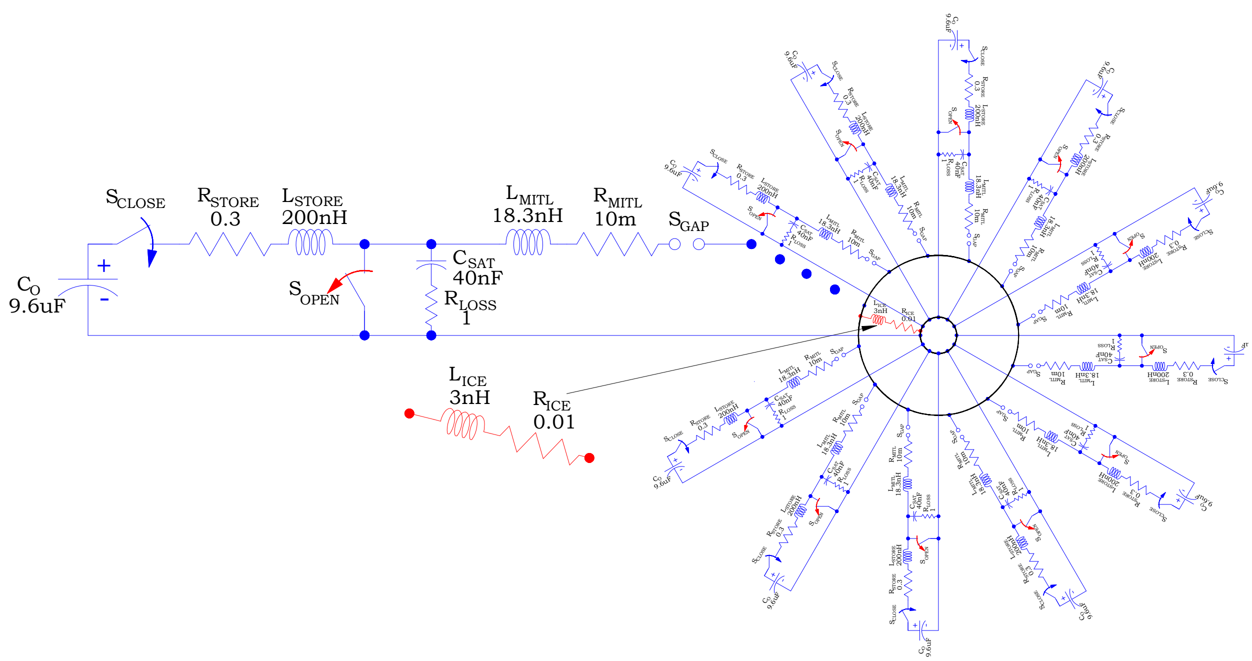

Fig. C4. PSPICE model for the FEOS-ICE driver

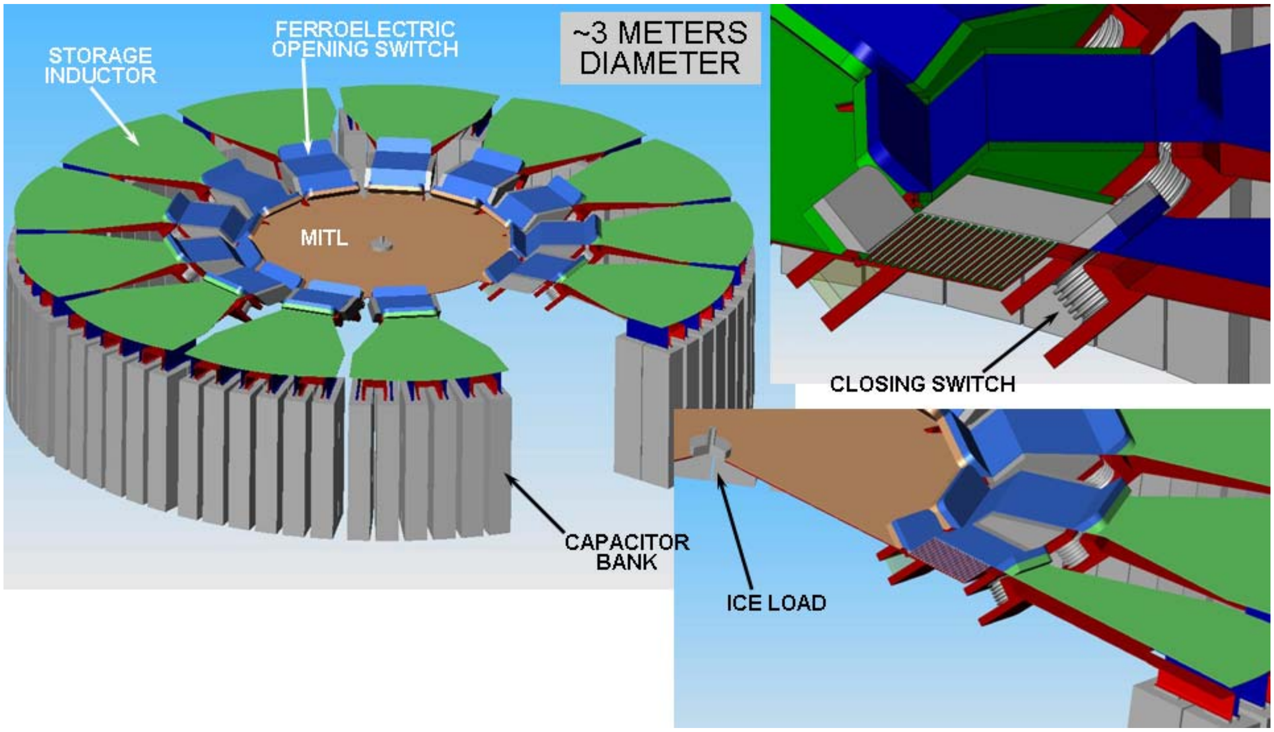

Fig. C5: Conceptual FEOS based ICE Driver Hardware.

APPENDIX D: Mechanical &Thermal model used in this paper for determining heating, losses and mechanical reaction in the conductors of a MES.

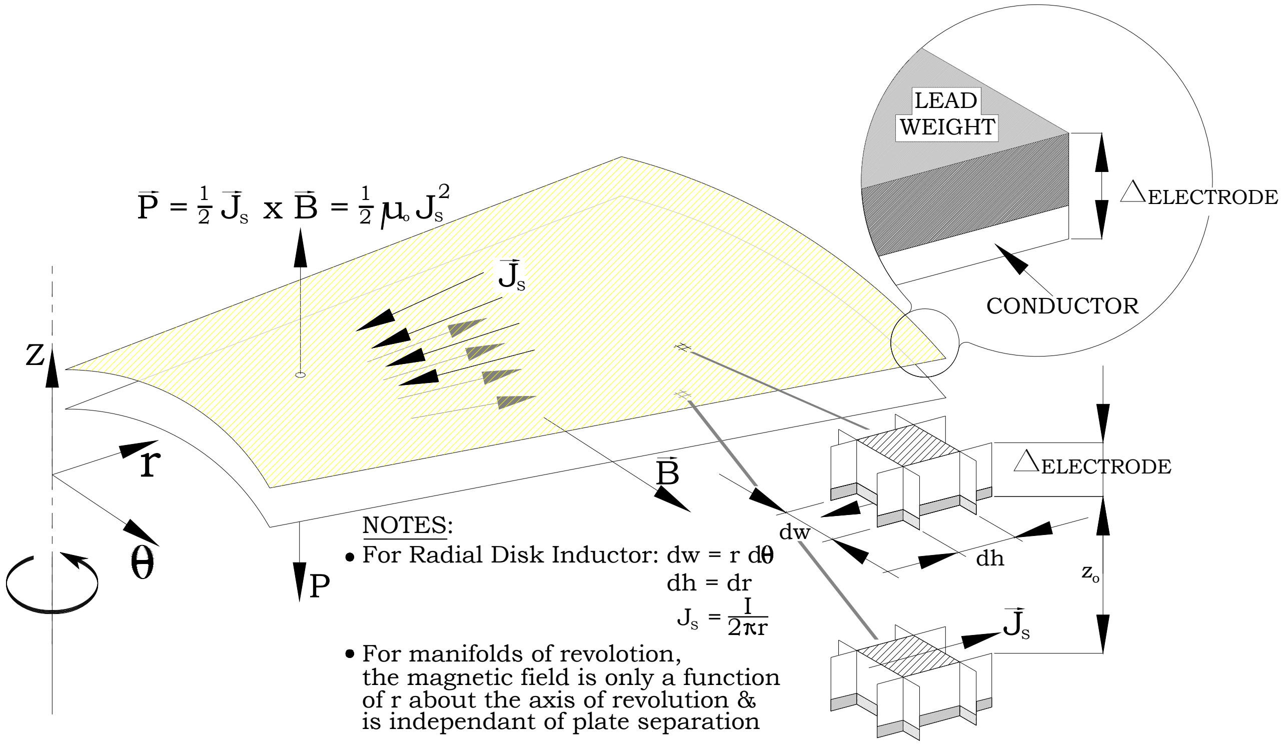

Fig. D1. A storage inductor that is a manifold of rotation about the load axis is applicable to the likely fusion driver topology

The Model: For a differential element, Fig. D1:

Electrical Equations:

- $J_S = J_o \sin(2\pi t/T_{CHARGE})/[1+(t/t_{OPEN})^{50}]$ (shuts off at $t_{OPEN} \approx$ ¼T) (D1)
- $\delta(t) = 2\,[t/(\pi\sigma\mu)]^{1/2} < \Delta_{ELECTRODE}$ (APPENDIX A) (D2)
- $\sigma(\theta) = \sigma_o/\{\zeta[1 + \xi(\theta - \theta_o)]$ (APPENDIX B, Table B1) (D3)
- $dE = di^2R = di^2[dh/(\sigma\ dw\ \delta)]\ dt = J_S{}^2 dw\ dh/(\sigma\delta)\ dt$ (D4)

where, T_{CHARGE} = period of the sinusoidal storage inductor charging time
δ = skin depth, which is the thickness of the differential element normal to the surface of the conductor. If it becomes greater than $\Delta_{ELECTRODE}$, it is replaced by $\Delta_{ELECTRODE}$.
$\Delta_{ELECTRODE}$ = electrode thickness
θ = temperature
θ_o = 20^{o}C
π = 3.141592654…
σ = electrical conductivity
di(t) = differential current flowing in the h direction in the element

dh = length of the differential element in the current direction
dw = width of the differential element transverse to the current in the plane of the conductor
dE = increase in the thermal energy in the differential element in time, dt
J_S = surface current density [current per unit width]
t_{OPEN} = the time that the opening switch opens

Thermodynamic Equations:

- $\rho = \rho_o/\{[1 + \beta(\theta - \theta_o)]^3\}$ (APPENDIX B, Table B2) (D5)
- $d\theta = dE/(mc_v) = dE/[(\rho\ dw\ dh\ \delta)c_v] = J_S^2/(\sigma\rho c_v\delta^2)\ dt$ (D6)

where, ρ = volumetric mass density, ρ_o is at θ_o & ρ is at θ
β = coefficient of linear expansion [(Δlength/length)/ ^{o}Temperature]
c_v = specific heat at constant volume (APPENDIX B, Table B3 [xi])

Thermal energy losses and temperature rise are calculated by integrating (4) & (6), respectively.

Dynamics Equations: [xii]

- $P = \frac{1}{2}\mu_o J_S^2$ (D7)
- $a = P/(\rho\ \Delta_{ELECTRODE})$ (D8)
- $\upsilon = da/dt$ (D9)
- $z = d\upsilon/dt$ (D10)
- $z_{MAX} \approx z(t_{OPEN}) + \frac{1}{2}\upsilon(t_{OPEN})^2/g$ (D11)

where, P = magnetic pressure
a = acceleration of the electrode normal to its surface
υ = velocity of the electrode normal to its surface
z = displacement of the electrode normal to its surface from its original position
$\Delta_{ELECTRODE}$ = electrode thickness, normal to its surface
z_{MAX} = maximum vertical displacement (ballistic)
z_o = initial transmission line electrode spacing, Fig. D1.
g = gravitational acceleration = 9.8 m/s^2

As a demonstration, these analyses were run with a current density that reaches a peak of 60 MA/m in 1 us and a 50 inch thick Tungsten electrode set. Temperature was limited to half the melting temperature. The results of the thermal analysis are shown in Fig. D2. The current waveform used corresponds to that which would flow in an RLC circuit with an initially charged capacitor and a series closing switch that closes at t = 0 and an opening switch that opens at

[xi] Specific heat goes up with temperature, but data for exactly how much was unavailable so it was treated as constant for a worst case solution.
[xii] We are treating the electrode as a rigid mass (worst case). Actually, for the small surface displacements that we are limiting the problem to, the energy will be absorbed in an acoustic wave that dissipates as it bounces between the electrode surfaces and propagates radially along the electrode due to the radial variation in pressure.

t_{OPEN} = 1 us, Fig. D3. The current in L_{STORE} builds up sinusoidally by being conducted through the ferroelectric opening switch back to the primary storage capacitor, C_o, Fig. D4. This is one way that and inductive energy store could be charged with current. The current abruptly drops to near zero when the opening switch opens, because the load is characteristically much more resistive than the opening switch in the ON state. After the current pulse is over, the top transmission line plate continues to move upwards ballistically to a much greater height than it was at when the current pulse stopped. The peak displacement is calculated from Eqn. D11.

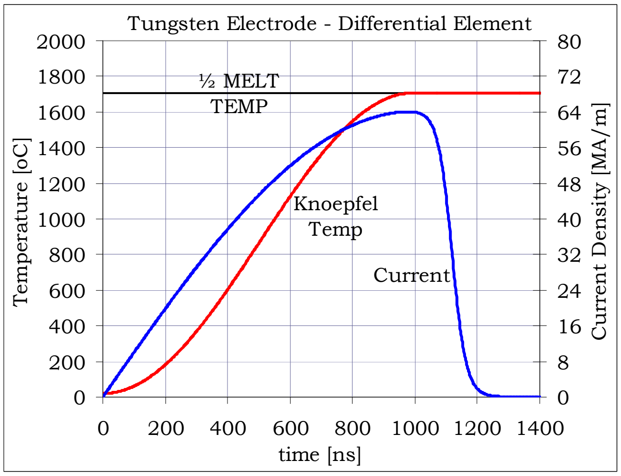

Fig. D2. Peak current density of 64 MA/m yields a rise to ½T_{MELT} in Tungsten.

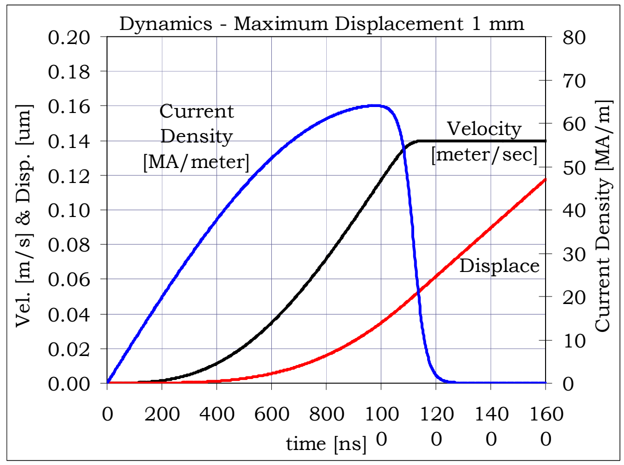

Fig. D3. 64 0MA/meter yields a velocity of 0.14 meters/sec & 1 mm displacement.

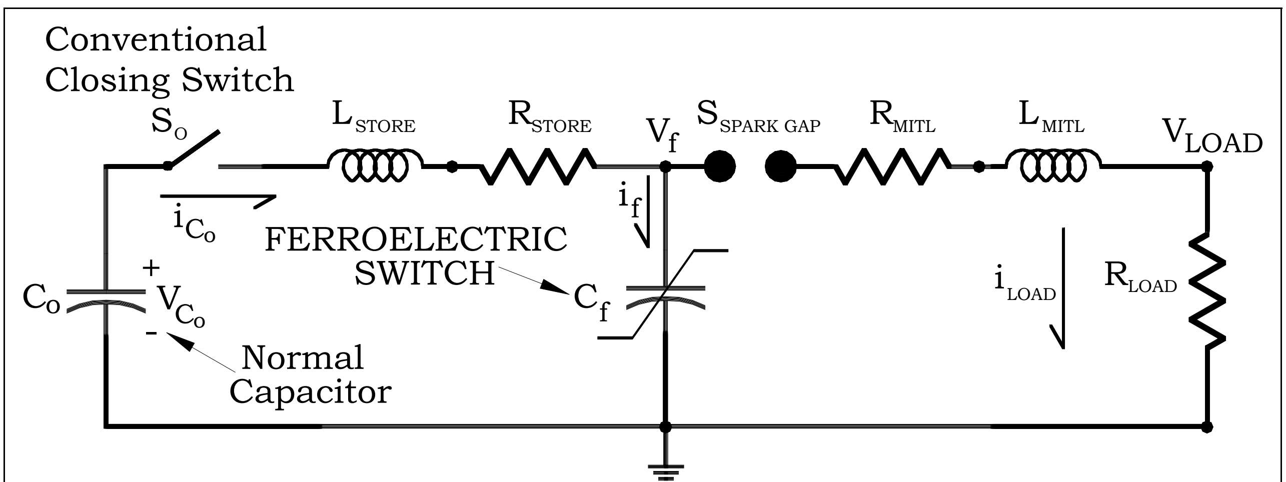

Fig. D4. Typical MES pulser circuit.

APPENDIX E: A model for a Hohlraum wire load.

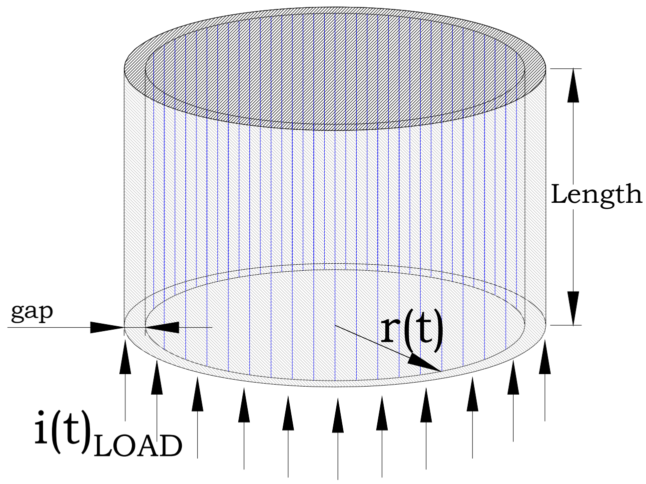

Fig. E1. Geometry of the Hohlraum used in the Dynamic Load Model.

Hohlraum Equations:

- $\text{Pressure} \bullet 2\ \ r = \frac{1}{2}\mu_o[i_{LOAD}/(2\ \ r)]^2 \text{ x } 2\ \ r$ (E1)
- $d^2r/dt^2 = \ \ /(4\ \ \ _L r)\ i_{LOAD}^2$ (E2)
- $dr/dt = \int d^2r/dt^2\ dt$ (E3)
- $r(t) = \int dr/dt\ dt + r(t=0)$ (E4)
- $L_{LOAD} = \ell\ (\mu/(2\ \ ))\ \ln[(r(t=0)+\text{gap})/r(t)]$ (E5)

where,

i_{LOAD}	=	current down through the Hohlraum load
$r(t)$	=	radial position of the wire array/plasma wall
ℓ	=	axial length of the Hohlraum array
gap	=	initial radial spacing between the Hohlraum wire array and the outer wall of the Hohlraum feed
ρ_L	=	mass per unit axial length of the wire array
L_{LOAD}	=	inductance of the load

The coaxial Hohlraum, Fig. E1, is modeled as a symmetrically imploding non-relativistic shell of metal plasma with a fixed mass and no Rayleigh-Taylor instabilities. Plasma mass is assumed to be conserved – no ablation. The array plasma stagnates when the original radius is reduced by the convergence ratio. Stagnation occurs when the outward thermodynamic pressure balances the inward magnetic pressure on the wire plasma. Upon stagnation, the load converts to a plasma resistor and an inductance that is decreasing, due to diffusion of the current through the plasma.

APPENDIX F: A model for the main P-E loop of a ferroelectric.

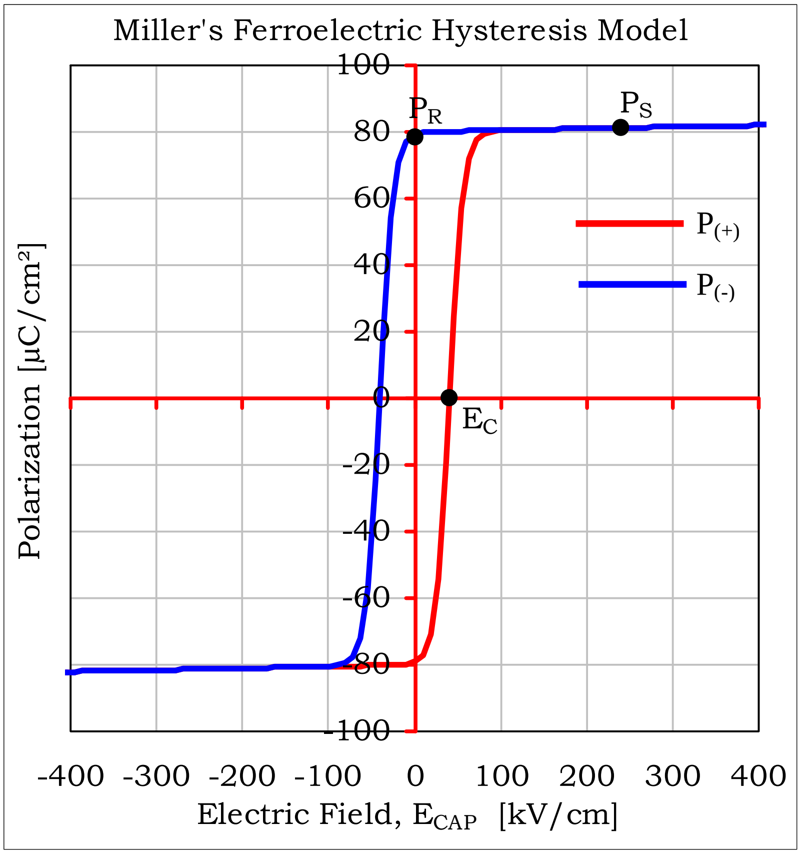

Fig. F1. Lithium Niobate ($LiNbO_3$), P-E Loop used for the modeling.

A typical P-E loop is shown in Fig. F1 with the key parameters noted. S. Miller proposed a fit to this constitutive relation that is expressed in terms of these key parameters. Note that this is only the major loop and does not account for minor loops.

Miller's Constitutive Model (Fig. 7) 22*:*

- $P_{(+)} = P_S \tanh[(E - E_C)/2\ \ ] + \ _o(\ _r -1)E_{CAP}$
  (F1)

- $dP_{(+)}/dE = P_S/[(2\ \ ) \cosh^2\{E_{CAP} - E_C)/2\ \ \}] + \ _o(\ _r -1)$ (F2)

- $P_{(-)} = -P_S \tanh[(-E - E_C)/2\ \ ] + \ _o(\ _r -1)E_{CAP}$ (F3)

- $dP_{(-)}/dE = P_S/[(2\ \ ) \cosh^2\{(-E - E_C)/2\ \ \}] + \ _o(\ _r -1)$ (F4)

- $\ \ = E_C/\ln[(1+P_r/P_S)/(1-P_r/P_S)]$ (F5) *where,*

P(+) = macroscopic polarization when the electric stress is increasing
P(-) = macroscopic polarization when the electric stress is decreasing
E = applied electrical stress
E_C = the coercive electric field
P_S = "spontaneous" polarization (see Fig. F1)

Some typical parameters for common ferroelectric materials are given in Table F1.

Table F1. Typical material parameters for some common ferroelectric materials.

	Best Commercially Available High-Voltage Capacitor [xiii]	Typical Commercial High-Voltage Transducer [xiv]	Best Projected Option for Single-Shot Operation [xv]	Best Projected Option for Repetitive Operation [xv]	Best Projected Achievable from Textured Poly-Crystalline Short-Term [~1yr] [xvi]	Best Projected Achievable from Textured Poly-Crystalline, Long-Term [~3yr] [xvii]	Measured
	$BaTiO_3$ - Based	*PZT 5A*	*$LiNbO_3$*	*$LiTaO_3$*	*$PbTiO_3$ -based*	*$BiFeO_3/Bi(Zn,Nb)O_3 – PbTiO_3$*	
$\varepsilon_{r(SAT)}$	150	100	30	40	100	200	30
P_S [$\mu C/cm^2$]	16	41	80	55	70	110	48
P_R [$\mu C/cm^2$]	9	37	79	53	65	100	47.9
E_C [kV/cm]	10	12	40	1	18	~50-150(?)	11

The best possible ferroelectric for opening switches are:

Category I: Desirable P-E characteristics

- $P_R \approx P_S$ because this yields the most square cornered P-E loop which yields the greatest contrast between the impedance of the switch in the unsaturated state and the impedance of the switch in the saturated state. A nearly vertical unsaturated loop section means that it will be a good short in the ON-state. A nearly horizontal saturated loop section means that it will present very high impedance in the OFF-state.

- $P_S \rightarrow \infty$ because this yields the smallest required switch area for a given conduction time. The switch opens when the charge injected equals the ferroelectric's capacity to compensate for the injected charge on the electrodes by flipping polarizations (see APPENDIX H). In short, if you double the spontaneous polarization, then the switch can be aerially half as large to accept a given Coulomb transfer before opening.

[xiii] Values estimated from common BaTiO3-based high-voltage capacitors; consistent with those used in the previous FEOS papers.
[xiv] Piezoelectric strain could be a problem.
[xv] This is a stoichiometric crystal.
[xvi] Materials available, would require processing development to fabricate them with optimized properties.
[xvii] This would require both chemical and processing optimization to fabricate materials with such properties

- $E_C \rightarrow 0$ dielectric losses per unit volume are the area inside the P-E loop as the system traverses the loop while operating, so lower coercive fields will yield lower losses.

$$dW/dV = \int_P \underline{E}\bullet d\underline{P} \quad \textit{loss per unit volume} \qquad \text{(F6)}$$

- Lower $\varepsilon_{r(SAT)}$ yields faster rise times and higher voltages into an inductive load. The current rise time into an inductive load is essentially the time it takes for the storage current to charge the linear capacitance of the ferroelectric switch after it is saturated. So, small is good, but if this linear capacitance is *too* small then the voltage on the switch will go to high and break it.

Category II: We didn't think about these characteristics until we did the experiments:

- Must massively and instantly volumetrically nucleate domains when an electrical stress that is much less than the break-down field is applied. The nucleation sites must be close enough together so that the domain boundaries will close on one another throughout the entire volume of the switch in a time frame that is much shorter than the time that the storage inductor will be charged with current[xviii]. *We found that single crystal materials will not massively nucleate when an electrical stress is applied.*

- The piezoelectric coefficient must not be so large that the switch mechanically self destructs when subjected to MV/cm-scale electrical stresses with risetimes on the order of 1 ns to 1000 ns.

- Must be very durable. *Single crystals tend not to be.* In a practical laboratory setting, these switches are subject to a lot of rough treatment. Even if they are installed gently, the mechanical shock that hits the switch during a shot can be substantial. It is necessary to make extremely good electrical contact which can entail clamping the switch material between electrodes with very high pressures.

- High electrical strength. These materials must be able to repeatedly withstand electrical stresses of 1 MV/cm to several MV/cm with durations of several tens of nanoseconds. This is the kind of electrical stress that the switch is subjected to during the time that energy is being delivered to the load.

Single crystal Lithium Niobate ($LiNbO_3$) is one of the most suitable materials for the opening switch application from the Category I standpoint because it has a low coercive field, high spontaneous polarization and its dP/dE characteristic transitions from nearly vertical in the unsaturated state to nearly horizontal in the saturated state. Conversely, single crystal lithium niobate fails in Category II, because it won't instantly volumetrically nucleate when a high electric field is applied and it is brittle.

[xviii] Domain walls move at less than the speed of sound in the material with a velocity that depends upon the material and amplitude of the electrical stress applied.

APPENDIX G: Pulser circuit model with a dynamic load, Fig. G1.

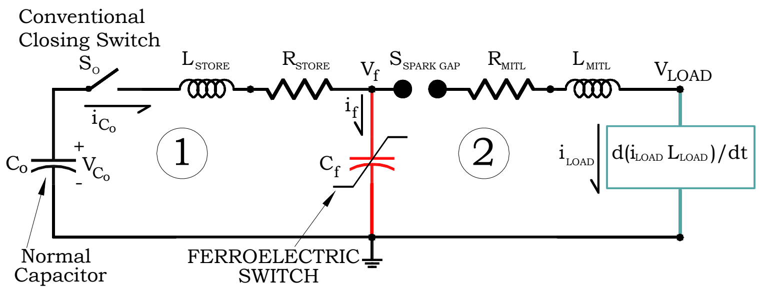

Figure G1. Model used for the single stage Ferroelectric Inductive Energy Storage Driver.

Circuit Equations:

- $v_{Co} = \int(dv_{Co}/dt)\,dt + v_{Co}(t=0)$ (G1)
- $dv_{Co}/dt = -i_{Co}/C_o$ (G2)
- $i_{Co} = \int di_{Co}/dt\,dt + i_{Co}(t=0)$; $i_{Co}(t=0) = 0$ (G3)
- $di_{Co}/dt = (v_{Co} - v_f - i_{Co} R_{STORE})/L_{STORE}$ (G4)
- $v_f = \int dv_f/dt\,dt + v_f(t=0)$: $v_f(0)=0$ to start at negative P_r (G5)
- $dv_f/dt = i_f/[A_{CAP}(\ \ _o/d_{CAP} + dP/dv_f)]$
  $= i_f/[A_{CAP}(\ \ _o/d_{CAP} + (1/g)dP/dE)]$ (G6)
- $i_{LOAD} = \int di_{LOAD}/dt\,dt + i_{LOAD}(t=0)$ (G7)
- $di_{LOAD}/dt = (v_f - i_{LOAD}(R_{MITL}+dL_{LOAD}/dt))/(L_{MITL}+L_{LOAD})$
  (G8)
- $i_f = i_{Co} - i_{LOAD}$

where,

	v_{Co}	= voltage on the primary storage capacitor
	i_{Co}	= current out of the positive terminal of the storage capacitor
	v_f	= voltage on the top of the ferroelectric switch
	i_f	= current down through the ferroelectric switch
	i_{LOAD}	= current down through the Hohlraum load
	v_{LOAD}	= voltage on the top of the Hohlraum load
	$r(t)$	= radius of the wire Hohlraum array
	P	= dielectric polarization
	E	= electric field in the switch
	g	= switch electrode spacing
	A_{CAP}	= area of the ferroelectric switch
	C_o	= storage capacitor
	R_{STORE}	= resistance of the storage inductor
	L_{STORE}	= inductance of the storage inductor
	L_{MITL}	= inductance of the MITL feed
	R_{MITL}	= MITL feed resistance
	L_{LOAD}	= Hohlraum inductance
	P	= net polarization of the ferroelectric switch
	ε_o	= permittivity of vacuum

APPENDIX H: How to program when the FEOS opens.

The switch state changes when the injected charge reaches the switches capacity to hold it,

$$\int_0^{t_{SWITCH}} i(\zeta)\, d\zeta = \iint_{S_{ELEC}} \mathbf{P}_S \bullet d\mathbf{S} - q_o \qquad \text{(I1)}$$

where,

$i(t)$ =	primary inductor charging current	[A]
$\mathbf{P}_S$ =	spontaneous surface polarization vector	[nC/cm^2] [xix]
t_{SWITCH} =	time that the switch opens	[s]
S_{ELEC} =	surface of the smallest electrode	[cm^2]
$d\mathbf{S}$ =	incremental normal surface vector	[cm^2]
q_o =	initial charge placed on the switch	[Coul]

Switch timing jitter is the same as that for the primary inductor charging source, which can be made on the order of ~1 ns. Switch timing, t_{SWITCH}, can be controlled by the initial charge that is placed on the switch - which behaves like a capacitor for this purpose.

[xix] Spontaneous polarization is due to complete domain alignment. Saturation polarization includes linear dipole stretching.

References:

1. R. J. Commisso, P. J. Goodrich, J. M. Grossmann, D. D. Hinshelwood, P. F. Ottinger, and B. V. *"Characterization of a microsecond-conduction-time plasma opening switch"* Weber, Phys. Fluids B 4 (7), July 1992, p. 2368-2376.

2. M.E. Savage, W.W Simpson & M.A. Usher, *"Results from Long Conduction Time Plasma Opening Switch Experiments at Sandia National Laboratories"*, 9th IEEE International Pulsed Power Conference, Albuquerque, New Mexico, 1993, pp. 110-114.

3. Hiroyuki Kida, *"Measured and Simulated Results of Impulse Generator Using Step Recovery Diode"*, IEICE Trans. Fundamentals, Vol.E88–A, No.9 September 2005, pp. 2381-2383.

4. Sol Schneider, Life Fellow, IEEE, and Thomas F. Podlesak, Member, IEEE, *"Reverse Switching Dynistor Pulsers"*, IEEE Transactions on Plasma Science, Vol. 28, No. 5, October 2000, pp. 1520-1523.

5. A. Gunther, M. Kristiansen and T. Martin, *"Opening Switches"*, Plenum Press, New York (1987),
pp. 6-8.

6. F. W. MacDougall, J.B. Ennis, R.A. Cooper, J. Bates, K. Seal, *"High Energy Density Pulsed Power Capacitors"* 2003 IEEE International Pulsed Power Conference, Digest of Technical Papers, IEEE Catalog Number 05CH37688C, pp. 513-517.

7. Fred MacDougall, Joel Ennis, Xiao Hui Yang, Ken Seal, Sanjay Phatak, Brian Spinks, Nathan Keller, Chip Naruo and T. Richard Jow, *"Large High Energy Density Pulse Discharge Capacitor Characterization"*, 2005 IEEE International Pulsed Power Conference, Digest of Technical Papers, IEEE Catalog Number 05CH37688C, pp. 1215-1218.

8. S. A. Nasar and H. H. Woodson, *"Storage and Transfer of Energy for Pulsed-Power Applications"*, Proceedings of the Sixth Symposium on Engineering Problems of Fusion Research, (1975), pp. 316-321.

9. Grenoble High Magnetic Field Laboratory, *"Quasi-Stationary Magnetic Fields Using Inductive Energy Storage"*, Technical Report

10. *S.* M. Schoenung, W.R. Meier, R. L. Fagaly, M. Heiberger, R. B. Stephens, J. A. Leuer, and R. A. Guman, *"Design, Performance, and Cost Characteristics of High Temperature Superconducting Magnetic Energy Storage"*, IEEE Transactions on Energy Conversion, Vol. 8, No**.** 1, March 1993, pp. 33- 39.

11. H. J. Niu and D. P. Hampshire, *"Disordered Nanocrystalline Superconducting PbMo6S8 with a Very Large Upper Critical Field"*, Physical Review Letters, Vol. 91, No. 2, July 2003, 027002-1 – 027002-4.

12. Y. B. Huang, X. Y. Cai, G. N. Riley, Jr., D. Larbalestier, D. Yu, M. Teplitsky, A. Otto, S. Fleshler and R. D. Parrella, *"Progress in BI-2223 Tape Performance"*, American Superconductor, Technical Papers.

13. W.A. Stygar, et al., "*Architecture of petawatt-class z-pinch accelerators,*" Physical Review Special Topics - Accelerators and Beams 10, 030401 (2007), pp. 1-24.

14. G.H. Rim, E. P. Pavlov, J.S. Kim, Kyung-Nam, Chang-won and Sung-Ju Dong, *"Nanosecond Pulse Generation with Nonlinear Capacitors and Magnetic Power Compression"*, 13th IEEE International Pulsed Power Conf. (2001).

15. Geun-Hie Rim, Hong-Sik Lee, Pavlov E. P., Won-Ho Kim, Chu-Hyun Cho, Young-Wook Choi, *"Fast high voltage pulse generation using nonlinear capacitors"*, 12th IEEE International Pulsed Power Conf., (1999), pp. 1460-1463.

16. Shinji Ibuka, Takehiro Miyazawa, Akira Ishii and Shozo Ishii, "*Fast High Voltage Pulse Generator with Nonlinear Transmission Line for High Repetitive Operation"*, 10th IEEE International Pulsed Power Conf. (1995), pp. 1365-1370.

17. Mark E. Savage, William A. Stygar, Juan M. Elizondo, Harry *C.* Ives, William Shoup, Kenneth W. Struve, Dillon H. McDaniel, *"Effect of Self-Magnetic Field on Large Pulsed Insulators Operated at 4 Megavolts and 5 Mega amperes"*, Conference Record of the Twenty-Sixth International Power Modulator Symposium 2004 and 2004 High-Voltage Workshop, pp. 54-59.

18. S.Yu. Kazakov, V.P. Yakovlev, A.D. Kanareykin, E.A. Nenasheva, and J.L. Hirshfield, *"700 MHZ Low-Loss Electrically-Controlled Fast Ferroelectric Phase Shifter for ERL Applications"*, Proceedings of PAC07, Albuquerque, New Mexico, USA, T28 Subsystems, Technology and Components, 1-4244-0917-9/07 2007 IEEE, pp. 599-601.

19. E. E. Jamieson, *"Ultrasonic Imaging for Poling"*, Honeywell Report KCP-613-6312, Published March 2000, Available from The National Technical Information Service, U. S. Department of Commerce, 5285 Port Royal Rd., Springfield, Virginia 22161, (703) 487-4650.

20. Yount-Han Shin, Ilya Grinberg, I-Wei Chen and Andrew M. Rappe, "*Nucleation and growth mechanism of ferroelectric domain-wall motion"*, Nature (Letters) nature 06165.3d 4/9/07, Fig. 2b.

21. S.L. Miller, J.R. Schwank, R.D. Nasby, and M.S. Rodgers, "*Modeling ferroelectric capacitor switching with asymmetric nonperioudic input signals and arbitrary initial conditions,"* J. Appl. Phys. 70 (5), 1 September 1991, pp. 2849-2860.

22. Heinz E. Knoepfel, "*Pulsed High Magnetic Fields: Physical Effects and Generation Methods Concerning Pulsed Fields up to MegaOersted Level,"* UMI Books on Demand, pp. 49-56

Distribution List:

5	MS 1152	Kim Reed, 1653
5	MS 1152	Joe Rudys, 1653
5	MS 1152	Steve Glover, 1653
5	MS 1152	Gary Peña, 1653
1	MS 1181	Larry Schneider, 1650
1	MS 1411	G. Brennecka, 1816
1	MS 1411	B. Tuttle, 1816
1	MS 0123	D. Chavez, LDRD Office, 1011 (electronic copy)
1	MS 0899	Technical Library, 9536 (electronic copy)

Sandia National Laboratories